HHS Public Access

Author manuscript

J Immunol. Author manuscript; available in PMC 2022 December 01.

Published in final edited form as:

J Immunol. 2021 December 01; 207(11): 2720–2732. doi:10.4049/jimmunol.2100208.

Thymus-derived CD4+CD8+ cells reside in mediastinal adipose tissue and the aortic arch

Holger Winkels[*,†], **Yanal Ghosheh**[*], **Kouji Kobiyama**[*], **William B. Kiosses**[*], **Marco Orecchioni**[*], **Erik Ehinger**[*], **Vasantika Suryawanshi**[*], **Sara Herrera-De La Mata**[*], **Paola Marchovecchio**[*], **Thomas Riffelmacher**[*], **Nicolas Thiault**[*], **Mitchell Kronenberg**[*], **Dennis Wolf**[‡], **Gregory Seumois**[*], **Pandurangan Vijayanand**[*], **Klaus Ley**[*,§]

[*]La Jolla Institute for Immunology, La Jolla, CA, 92037, USA

[†]Clinic III for Internal Medicine, Department of Cardiology, University of Cologne, 50937, Cologne Germany

[‡]University Hospital Freiburg, 79106, Freiburg, Germany

[§]UCSD Bioengineering, La Jolla, CA, 92093, USA

Abstract

Double-positive $CD4^+CD8\alpha\beta^+$ (DP) cells are thought to reside as T cell progenitors exclusively within the thymus. We recently discovered an unexpected $CD4^+$ and $CD8\alpha\beta^+$ immune cell population in healthy and atherosclerotic mice by single cell RNA-sequencing. Transcriptomically, these cells resemble thymic DPs. Flow cytometry and 3D-whole-mount imaging confirmed DPs in thymus, mediastinal adipose tissue (MAT), and aortic adventitia, but nowhere else. Deep transcriptional profiling revealed differences between DP cells isolated from the three locations. All DPs were dependent on RAG-2 expression and the presence of the thymus. MAT DPs resided in close vicinity to iNKT cells, which they could activate *in vitro*. Thymus transplantation failed to reconstitute extrathymic DPs and frequencies of extraythymic DPs were unaltered by pharmacologic inhibition of S1P1, suggesting that their migration may be locally confined. Our results define two new, transcriptionally distinct subsets of extrathymic DPs that may play a role in aortic vascular homeostasis.

Introduction:

Pro- and anti-inflammatory immune cells modulate the progression of atherosclerosis locally and systemically (1). We and others have recently utilized high-parametric methodologies, 10x Genomics based single cell RNA sequencing (scRNA-Seq) and mass cytometry (CyTOF) to define aortic leukocytes in non-atherosclerotic and atherosclerotic mice (2, 3). With both approaches, we identified the unexpected presence of a cell population, which did not express surface TCR but were $CD4^+$ and $CD8\alpha^+$ and $CD8\beta^+$.

Corresponding author: Holger Winkels, holger.winkels@uk-koeln.de, Twitter: @WinkelsLab, Phone +49-221-478-40897, Telefax +49-221-478-87327.

The only known cell population in the murine and human body harboring these features are $CD4^+CD8^+TCR^-$ (DPs), a progenitor stage of T cells found exclusively in the thymus, where the development of T cells takes place. In this process, bone-marrow derived progenitors migrate into the thymus and a portion of them differentiate into naïve single $CD4^+$ or $CD8^+$ TCRαβ expressing T cells (4). Recombinase activating gene (RAG) 1 and 2 catalyze the rearrangement of the V, D, and J TCRβ gene segments into a unique combination of a TCRβ chain. This chain will pair with an invariant preliminary alpha chain (*pTa*) to form a pre-TCR in conjunction with the CD3 complex. Pre-TCR signaling is necessary for thymocyte survival, proliferation, and blocks further β chain loci rearrangement. Simultaneously, the TCR co-receptors CD4 and CD8αβ co-emerge on the thymocyte surface to form double positive DP thymocytes. DPs start TCR alpha chain rearrangement and subsequently undergo positive selection, based on affinity for unknown self-peptides presented by major histocompatibility complexes (MHC). Following successful selection, one of the co-receptors (CD4 or CD8) will be downregulated based on the MHC-restriction of the TCR and naïve, mature MHC class II-restricted $CD4^+$ or MHC class I-restricted $CD8\alpha\beta^+$ T cells will emigrate into the blood, from where they reach secondary lymphoid organs like lymph nodes and spleen.

The present study was undertaken to test whether extrathymic DPs were specifically induced in atherosclerosis. We further aimed to fully characterize their transcriptomes, identify their relationship with immature DP thymocytes, assess their functionality, and their mode of migration.

Material and Methods

Mice

All experiments followed guidelines of the La Jolla Institute for Immunology (LJI) Animal Care and Use Committee. Approval for use of rodents was obtained from LJI according to criteria outlined in the Guide for the Care and Use of Laboratory Animals from the National Institutes of Health. All mice were maintained in-house on a 12-hour light/dark cycle and had excess to chow diet *ad libitum*. Female *C57BL/6J* (cat.# 000664), *CD45.1*$^+$ (*B6.SJL-PtprcaPep3b/BoyJ,* cat.# 002014), *BALB/cJ* mice (cat.# 000651), *Cd1d*$^{-/-}$ (C57BL/6-Cd1d1tm1.1Aben/J, cat.# 016929) and *Rag2*$^{-/-}$ (*B6(Cg)-Rag2*$^{tm1.1Cgn}$*/J,* cat.# 008449) were purchased from The Jackson Laboratory. If indicated, sham-operated or thymectomized *C57BL/6J* mice were also commercially obtained from The Jackson Laboratory. *Rag2*^{GFP} and *Cd1d*$^{-/-}$ mice were kindly provided by Dr. Kronenberg. *C57BL/6J* and *CD45.1*$^+$ were crossed to obtain *CD45.1/2* mice.

Mice at indicated ages were euthanized by CO_2 inhalation followed by blood withdrawal via cardiac puncture and perfusion with 10ml ice-cold PBS containing 100U/ml Heparin (Fresenius) before further organ and tissue dissection.

Aortic arch and mediastinal adipose tissue collection and processing

After perfusion, the chest of the mouse was opened and the thymus removed without damaging the capsule. Aortic arches and mediastinal adipose tissue were microsurgically

dissected and digested as previously described (5). Briefly, aortic arches and mediastinal adipose tissue pads were collected in 1ml RPMI medium (Thermo Scientific) containing 10% fetal bovine serum (FBS, Gemini) on ice. The collected tissue was cut into small pieces and individually digested for 1 hour at 37°C in HBSS containing 450U/ml Collagenase I (Milipore Sigma), 250U/ml Collagenase XI (Milipore Sigma), 120U/ml Hyaluronidase (Milipore Sigma), and 120U/ml DNase I (Milipore Sigma).

The digested tissue suspensions were subsequently filtered through a 50μm cell strainer (Partec) and washed with 37°C pre-warmed RPMI with 10% FBS at room temperature for 5min at 400xg. Cells were resuspended in pre-warmed RPMI with 10% FBS and incubated for 30min at 37°C to allow recovery of cell surface molecule expression affected during digestion. Cells were then washed and kept on ice either in PBS (Thermo Scientific) with 2% FBS for staining with fluorochrome-conjugated antibodies and flow cytometric analysis or in RPMI with 10% FBS for downstream processes.

Cell isolation from lungs

Both lobes of a lung were excised after perfusion and cut into small pieces, followed by the same digestion procedure applied to aortic arches and mediastinal adipose tissue. After digestion and rescue incubation, lung cells were kept on ice in PBS with 2% FBS for staining with fluorochrome-conjugated antibodies and flow cytometric analysis

Splenocyte isolation

Spleens were homogenized through a 70μm cell strainer (BD Biosciences), followed by washing with PBS and red blood cell lysis for 3min at room temperature using 1x RBC lysis buffer (Biolegend). Splenocytes were washed with PBS and kept in PBS with 2% FCS, and kept on ice for staining with fluorochrome-conjugated antibodies and flow cytometric analysis.

Thymocyte and lymphocyte isolation

Single cells suspension of thymocytes and lymph node residing cells were obtained by homogenizing the tissue through a 70μm cell strainer. The cell suspension was washed with ice-cold PBS and kept in PBS with 2% FBS on ice for staining with fluorochrome-conjugated antibodies and flow cytometric analysis.

Cell isolation from blood

Blood was withdrawn via cardiac puncture and collected in EDTA-coated tubes (Sarstedt). The plasma was removed after centrifugation for 5min at 400xg and 4°C. Erythrocytes were lysed using 1x RBC lysis buffer (Biolegend) for 10min at room temperature and the cell suspension was washed twice with PBS. Cells were kept in PBS with 2% FBS on ice for staining with fluorochrome-conjugated antibodies and flow cytometric analysis.

Cell isolation from small and large intestine

The intestine was dissected and surrounding fat pads and peyer’s patches were surgically removed. Small and large intestine were separated and both pieces were opened longitudinally and washed in RPMI containing 10% FBS and HEPES (2X, Thermo

Scientific). The intestinal compartments were cut into small pieces and collected in 30ml RPMI with 10% FBS and HEPES (2X, Thermo Scientific). Subsequently, EDTA (Milipore Sigma) and DTT (Milipore Sigma) were added to a final concentration of 5mM and 1mM, respectively. The suspension was incubated for 25min at 37°C while shaking at 250rpm and subsequently filtered through a 70μm strainer. After washing in PBS, the intestinal cell pellet was resuspended in 4ml of a 40% percoll gradient (GE Healthcare). The 40% percoll suspension was layered on top of 5 ml of a 60% percoll gradient (GE Healthcare) and centrifuged at room temperature at 900xg for 25min without acceleration and brake. The cell layer at the interphase was collected, washed with PBS, and kept on ice for staining with fluorochrome-conjugated antibodies and flow cytometric analysis.

Cell isolation from liver

The liver was dissected and homogenized through a 100μm cell strainer (BD Biosciences). After washing in PBS, the liver cell pellet was resuspended in 4ml of 40% percoll. The liver percoll suspension was carefully layered on top of 5ml 60% percoll solution and centrifuged at 900xg for 25min without acceleration and brake. The cell layer at the interphase was collected, washed with PBS, and kept on ice for staining with fluorochrome-conjugated antibodies and flow cytometric analysis.

Flow cytometry

Single cell suspensions were incubated with 50μl PBS containing 2% FBS, 10% rat serum (Milipore Sigma) and 10μg/ml anti-CD16/CD32 antibody (FC shield, clone 2.4G2, Tonbo Biosciences, cat. # 70–0161-M001) and live/dead staining (1:1000, either Thermo Scientific or Tonbo Biosciences) for 5min. Subsequently, 50μl PBS containing 2% FBS, 10% rat serum, 10μg/ml FC shield, live/dead staining (1:1000) and fluorochrome-conjugated antibodies (2x) were added for 20min on ice in the dark. Clones and final concentrations used are listed in Table S1. After incubation, cells were washed with ice-cold PBS containing 2% FBS. For determining cell proliferation, cells were fixed and permeabilized using the FoxP3 Transcription Factor Staining Buffer Set (Thermo Scientific) and stained with anti-Ki67-AF700 for 30min on ice and washed. If needed, samples were fixed with 2% Paraformaldehyde (PFA, Electron Microscopy Sciences) for 10min at room temperature. Cells were washed, resuspended in PBS containing 2% FBS, and acquired with a LSRII flow cytometer (BD Biosciences), LSRFortessa (BD Biosciences) or Amnis Imagestream (Milipore).

Fluorescence activated cell sorting (FACS sorting)

For FACS sorting, cells were stained as previously described. Before sorting, cells were kept in PBS containing 2% FBS and 2mM EDTA. Viable $CD4^{+}CD8^{+}TCR^{-}DUMP^{-}$ (DP) cells were sorted with a 70μm nozzle using the BD FACSAria Fusion and the FACSAria II cell sorter (both BD Biosciences). For imaging analysis, cells were sorted directly on Poly-L-Lysine glass (Milipore Sigma). For low-input sequencing, 400 DPs were sorted into low absorbent micro-centrifuge tubes (0.2ml, Eppendorf) containing 8μl low input lysis buffer containing recombinant RNAse inhibitor (40U/ul, CloneTech), dNTPs (Thermo Scientific), and 0.1% Triton X-100 (Thermo Scientific). For fetal thymic organ cultures,

cells were sorted into low absorbent micro-centrifuge tubes (1.5ml, Eppendorf) containing RPMI supplemented with 10% FCS.

Clearing and staining of whole mount tissue

Whole mount aortic arch, mediastinal adipose tissue, and thymus were fixed in Cytofix (BD Biosciences) 1:3 diluted in PBS overnight. The tissue block was washed in PBS for a day and blocked with 1% mouse serum (Milipore Sigma), 1% BSA (Milipore SIGMA), 0.3% TritonX-100 in PBS for 24h at room temperature while agitating. Subsequently, primary fluorescently conjugated antibodies were added 1:100 for 72h at 37°C in the dark while agitating. Hoechst (Thermo Scientific) was added at a concentration of 1:1000 for the final 2h. After staining, the whole mount tissue block was washed in PBS with 0.2% Triton X-100 and 0.5% 1-Thioglycerol (Milipore Sigma) overnight at room temperature. The buffer was replaced twice. C_e3D clearing solution (6) was freshly prepared as follows:

1ml contained 400µl (40%) N-methylacetamide, 1µl of Triton X-100 (0.1%), 5µl 1-Thioglycerol (0.5%) (all obtained from Milipore Sigma). For optimal solvation of all reagents, the buffer was shaken at 37°C for several hours. The whole mount tissue was removed from the washing buffer, carefully dried, and transferred into the clearing solution overnight at room temperature in the dark. The following day, the cleared whole mount tissue was mounted between two 1.5 borosilicate glass coverslips in clearing medium.

Staining of MAT for DPs and iNKT cells

Two pads of mediastinal adipose tissue were kept in 500µl PBS with 2% FCS and 1:100 of 10µg/ml anti-CD16/CD32 antibody (FC shield, clone 2.4G2, Tonbo Biosciences) at room temperature. The tissues were washed twice for 5min in PBS with 2% FCS. The mediastinal adipose tissue pads were incubated in 500µl PBS with 2% FCS and 1:100 CD4 A488 (clone RM4-5), 1:100 CD8α PE-Dazzle594 (clone 53–6.7) and either 10µl alpha-GalCer:CD1d-tetramer conjugated with A647 (40683, PBS-57, 1.6 mg/ml) or empty control CD1d tetramer conjugated with A647 (40684, 1.5 mg/ml). Samples were kept shaking overnight at 4°C and washed twice in PBS with 2% FCS. Nuclei were stained with 1:1000 Hoechst PBS with 2% FCS for 1h at room temperature. Samples were washed twice for 5 min in PBS with 2% FCS and fixed with 4% PFA for 1h. Samples were washed twice, mounted in Prolong Gold Mounting Medium (Thermo Scientific) and cured overnight with clamps and sealed with nail polish.

Imaging of whole mount tissue

Images were acquired at room temperature with a Zeiss LSM880 confocal microscope equipped with a 20x air objective (numerical aperture, 0.8) and Zen browser black v. 2019. Images used for 3D reconstructions were acquired at 405nm, 488nm, 561nm, and 633nm excitation wavelengths to visualize $CD31^+$ stained vessels single $CD4^+$, single $CD8^+$, and $CD4^+CD8^+$ cells. Spectrally tuned detectors were used to detect fluorescent signals and to minimize the overlap of fluorescent signals (greater than 660nm; 600–650nm; 499–553nm; 412–475nm). Main beam splitters were set at 405/488/561/633nm and a secondary beam splitter at 660nm. Signal from AF647 was directed to the AiryScan detector operated in confocal mode, and the signals from the other fluorochromes were read out using internal

detectors (405nm – Ch1 – bialkali PMT (725V); 488nm – ChS1 – GaAsP (800V); 561nm – far red detector Ch2 (720V); 633nm – ChA (700V)). The pinhole width was set at 24.6μm for all channels (= 0.49, 0.52, 0.61, 0.73 Airy Units, respectively.). Images were acquired at 5μm Z-step size and a pixel size of 0.42μm. 36 tiles were stitched together for a total image size of 5.13×5.53mm and a depth of 100μm (total pixel size: 12365×13320). Acquisition was performed in line-switching mode and unidirectional at a pixel dwell time of 0.77μs. Image analysis was performed in Imaris v.9.6 (Bitplane). Contrast stretching was used to increase visibility of image features (gamma = 1.0). Isosurfaces were generated based of nuclear signal. Fluorescence signal thresholds were obtained from control tissue to determine a filtering cutoff. This particularly was used to filter out autofluorescence from collagen fibers in the aortic arch. Cells were further filtered for sphericity with a cutoff of 0.7. A fluorescent image and an image generated after isosurface generation and filtering are displayed to demonstrate extrathymic occurrence of CD4CD8 double-positive cells.

Imaging of mediastinal adipose tissue and image reconstruction

Mediastinal adipose tissue Images for this tissue were acquired using a C-Apo 40w (1.2na) objective using as described a Zeiss LSM880 confocal microscope equipped with Gallium Arsenide Phosphide (GaAsP) detectors and Zen browser black v. 2019. Here on average 45 stacks of images per sample area were acquired at 0.5μm Z-step size and a pixel size of 0.129μm.

Imaging of sorted DPs

Viable DPs cells were isolated by FACS sorting from the thymus or mediastinal adipose tissue with aortic arch. Cells were directly sorted on a Poly-L-Lysine slide (Milipore Sigma). Up to 10000 cells were sorted in a spot placed on the glass slide. After sedimentation, sheath flow was removed and replaced with 4% PFA for 3 min. Subsequently, cells were washed twice with distilled water before mounting with fluorescent mounting gold medium (Thermo Scientific). After curing overnight, images were acquired at room temperature with the Zeiss LSM780 confocal microscope with a 63x oil objective (numerical aperture, 1.4) and Zeiss Zen browser black v. 2019.

Images were acquired at 405nm, 488nm, and 633nm excitation wavelengths. Spectrally tuned GaAsP detectors were used to detect fluorescent signals and to minimize the overlap of fluorescent signals (419–472nm, 508–543nm, 668–694nm, 650–694nm). Main beam splitters were set at 405/488/561/633nm and the signals were read out using internal detectors (ChS1 – GaAsP for all fluorochromes). For thymic cells, detector gains were set at 915 (Hoechst), 1069 (AF488), 1068 (PerCP), and 1007 (AF647), whereas extrathymic-isolated DPs were acquired at a gain of 782 (Hoechst), 1015 (AF488), 1091 (PerCP), and 930 (AF647). The pinhole width was set 1 Airy unit for all channels (= 43μm, 50μm, 58μm, 64μm, respectively). Images were acquired at a pixel size of 0.055μm (total pixel size: 1024×1024) and a Z-step depth of 0.374μm (total depth 4.12μm). Acquisition was performed in frame-switching mode and unidirectional at a pixel dwell time of 6.3μs.

EdU injection

8-week-old female *C57BL/6J* mice were injected intraperitoneally with 1mg EdU (Thermo Scientific) in PBS. Mice were sacrificed at days 1, 3, 5, and 7 post injection. EdU incorporation into DPs was assessed by the Click-IT EdU plus flow cytometry kit (Thermo Scientific) according to the manufacturer's instruction.

FTY720

FTY720 (Sellcheck) was dissolved in DMSO (Milipore Sigma) at 2mg/ml and stored at −20°C. The stock solution was diluted in sterile PBS supplemented with 3% BSA. 8-week-old female *C57BL/6J* were intraperitoneally injected at 1mg/kg body weight every day for 7 days. Alternatively, mice were injected with DMSO only.

Thymectomies

Female *C57BL/6J* mice were thymectomized three and 21 days after birth at The Jackson Laboratory before shipment to the La Jolla Institute for Immunology animal facility.

Kidney capsule transplantation

Female *C57BL/6J* mice were thymectomized or sham operated 21 days after birth at The Jackson Laboratory before delivery to the La Jolla Institute for Immunology. At the age of 10 weeks, mice were anesthetized with isoflurane and kept in deep anesthesia. A sterile field was prepared and the mouse kept on a heating pad to prevent hypothermia. Fur was removed from the left flank and the skin was prepared antiseptically. A small incision was performed into the skin and the window was opened to gain access to the peritoneum. The peritoneal cavity was opened close to the left kidney. The kidney was exposed and kept moist in saline. Using a microdissecting microscope and microsurgery tools (F.S.T.), a small incision was made into the kidney capsule into which one third of a thymic lobe of a congenically marked, female CD45.1 mouse was transplanted. After successful implementation of the thymic piece, the incision in the kidney capsule was sealed with tissue adhesive glue (Vetbond) and the kidney was returned into the peritoneal cavity. The peritoneal cavity and subsequently the skin were closed with 4–0 sterile and absorbable Vicryl sutures (Ethicon). Transplanted mice received an intraperitoneal injection of burprenorphine (0.1mg/kg body weight) and recovered in a temperature-controlled chamber at 37°C before being transferred into a sterile new cage. Mice were injected with a second dose of burprenorphine 4h later and monitored for their behavior daily during the first four days. Sutures were removed 10 days post-surgery and mice were euthanized for organ and tissue collection 21 days post-surgery.

Fetal thymic organ culture

DPs were FACS sorted from mediastinal adipose tissue and aortic arches of 8-week-old female *C57BL6/J* mice. Cells from 3–4 donor mice were pooled. The cell count was adjusted to 1×10^6/ml with pre-warmed DMEM with Glutamax (Thermo Scientific) and 10% FBS. Individual wells of a Terasaki plate (Milipore Sigma) were filled with 20μl cell suspension.

CD45.1 and CD45.2 mice were bred and plug formation of pregnant females was monitored. At E14, the uterus of pregnant mice was aseptically removed and transferred into a 90-mm petri dish (Milipore Sigma) containing DMEM with Glutamax and 10% FBS and embryos were removed. Single embryos were washed additionally in DMEM with Glutamax and 10% FBS to remove blood. Thymic lobes of E14 embryos were carefully removed from the chest cavity under a dissecting microscope and kept on ice in DMEM with Glutamax and 10% FCS. A single thymic lobe was added to a well in the Terasaki plate containing the cell suspension. Subsequently, the Terasaki plate was carefully inverted to allow migration of extrathymic DPs into the fetal thymus for 48h at 37°C and 5% CO_2. Subsequently, thymic lobes were collected and individually transferred on top of a transwell-filter in submersion culture for another 7 days at 37°C and 5% CO_2. At the end of the culture, thymic lobes were homogenized through a 50μm filter to obtain a single cell suspension which was prepared for flow cytometric analysis as previously described.

Glycolipid antigen presentation assay

Viable DPs cells were isolated by FACS sorting from the thymus or mediastinal adipose tissue with aortic arch from 8-week-old female *C57BL/6J* mice. Duplicate of cells (10k–250k) were cultured with 100ng/ml alpha-GalCer (BioVision, Milpitas, CA, USA) or left untreated in Dulbecco's modified Eagle's medium containing 10% FCS, 100 U/ml penicillin, 100 U/ml streptomycin, 2 mM L-glutamine, 1 mM sodium pyruvate, and 10 mM HEPES (all Thermo Scientific) with 10ng/ml IL-7 (R&D Systems, Minneapolis, MN, USA) for 3.5h at 37°C and 5% CO_2. Cells were washed twice with T cell medium and co-cultured with 50k iNKT DN3A4-1.2 hybridoma cells (7) for 12h in presence of IL-7. The supernatant was analyzed for IL-2 by ELISA while the cultured cells were prepared for flow cytometric analysis of CD69 surface expression.

Single sample Gene Set Enrichment Analysis

Single cell transcriptomes of aortic leukocytes isolated from atherosclerotic and non-atherosclerotic mice (GSM2882367: 8-week-old male, $Ldlr^{-/-}$ mice fed 11 weeks western-type diet; GSM2882368: 8-week-old male $Ldlr^{-/-}$ mice fed chow diet for 11 weeks; 8-week-old male $Apoe^{-/-}$ mice fed chow diet; 8-week-old male $Apoe^{-/-}$ mice fed chow diet for 12 weeks; 8-week-old male $Apoe^{-/-}$ mice fed western-type diet for 12 weeks) were integratively analyzed with Seurat. Batch correction was performed. The top 100 genes of the newly identified cell subset were extracted and subjected to a single sample gene set enrichment analysis (8, 9) of immune cell transcriptomes (GSE109125) isolated from bone marrow, spleen, and thymus. The enrichment score is reported as spider plot.

Low-input bulk RNA sequencing

For full-length transcriptome using Smart-Seq2, we followed a previously described protocol (10). In brief, 400 DPs were isolated by FACS sorting from aortic arch, mediastinal adipose tissue and thymus directly into 8μl low-input lysis buffer containing 0.1% Triton X-100, 10mM dNTPs, and 40U/μl recombinant RNAse Inhibitor in molecular grade water. We sorted at least 3 technical duplicates from pooled arch, mediastinal adipose tissue, or thymus cell suspensions of 5 female, *C57BL/6J* mice. Samples were vortexed, centrifuged at 3000xg for 2min, and stored at −80°C until further processing. To generate cDNA, we PCR-

amplified 4 μl of lyzed cells (equalling 200 cells) with 18 PCR cycles to obtain sufficient material for downstream procedures. The amplified cDNA was size selected and left-over primers eliminated through a magnetic beads dsDNA capture using a 0.8:1 vol:vol AMPure XP beads (Agencourt) procedure. Size selected cDNA was quantified with a fluorometric DNA quantification assay (PicoGreen dsDNA, ThermoScientific). 1 ng of cDNA was used to generate barcoded Illumina sequencing libraries using a standard tagmentation protocol (Nextera XT library preparation kit, Illumina; 9 cycles of PCR-based amplification using unique dual-index Illumina adaptors). As previously described, libraries were purified with a double size-selection protocol (0.5 followed by 0.8 volume bead/initial sample volumes), quantified (Picogreen quantification assay, Thermofisher) and fragment size measured by capillary-electrophoresis (Fragment analyzer, Advance analytical).

Samples failing our stringent quality control checks (quantity and size) were eliminated from further downstream steps (10). Libraries were pooled at equimolar ratios, quantified by qPCR assay (KAPA SYBR® FAST qPCR Kit - Roche), and sequenced using the Illumina sequencing platform and reagents. HiSeq2500 High output v4 (HiSeq SBS Kit v4, Illumina) libraries were sequenced for 50-bp single end reads. Post-sequencing, stringent quality controls were applied and samples that failed quality control checks were eliminated from further analysis (10). Samples were sequenced to obtain at least 8 million uniquely mapped reads.

Low-input RNA-seq mapping

All samples passed basic quality check through FASTQC v0.11.5 (11). Then, FASTQ files were mapped using STAR v2.6.0c (12) based on ENSEMBL reference GRCm38 and ENSEMBL mouse annotation release 92 (13). Gene counts were directly obtained from STAR using the parameter --quantMode GeneCounts. Post-mapping quality check was done though QoRTs v1.3.0 (14) with additional parameter --genomeBufferSize 50000. All commands were run using the UNIX command parallel v20161222 (15).

Processed sequencing data are available at the National Center for Biotechnology Information Gene Expression Omnibus repository (GSE180582).

https://www.ncbi.nlm.nih.gov/geo/query/acc.cgi?acc=GSE180582

Differentially expressed and co-regulated genes

Differential expression was done using DESeq2 v1.24 (16) according to the recommended workflow. Aside from 5 technical replicates which were clearly outliers according to their Euclidean distance to other technical replicates, all other technical replicates were collapsed using the DESeq2 function (collapseReplicates). Only genes which had a total of at least 10 reads across all samples were retained. No log fold change shrinkage was done. Adjustment for p-values was based on FDR (False Discovery Rate). Significantly differentially expressed genes were those with an adjusted p-value <= 0.05. Upset (17) was used to visualize set intersections between the various differentially expressed gene lists. Co-regulated genes were analyzed using WGCNA v1.68 (18) and was based on recommended workflow, with specific parameters (power = 9, TOMType = signed, corType = bicor, networkType = signed hybrid). TCR clonotypes were determined with MiXCR (19).

Statistical analysis

Data were routinely shown as mean with standard deviation. Unless stated otherwise, statistical significance was determined by Student's *t* test or analysis of variance (ANOVA) using Prism 8.1.2 (GraphPad). A value of more than three SDs from the mean served as criterium to exclude outliers.

Results:

$CD4^+CD8^+$ cells in the mediastinal adipose tissue and aortic adventitia

In silico analysis and integrative assessment of single cell transcriptomic data from aortic leukocytes sets derived from *Apolipoprotein E*-deficient mice (aged 8 weeks, aged 20 weeks and fed chow diet, aged 20 weeks and fed high fat diet for 12 weeks) and *low-density lipoprotein receptor*-deficient mice (aged 19 weeks and fed chow diet, aged 19 weeks and fed high fat diet for 11 weeks) showed $CD4^+$ and $CD8\alpha\beta^+$ double positive (DP) T cells in all five data sets (Fig1. A). To determine the relationship with other immune cells, we tested enrichment of the top100 genes of DP cells (Table S1) among bulk transcriptomes of various stem cell populations, thymic T cells progenitors, and splenic naïve $CD4^+$ and $CD8\alpha\beta^+$ T cells. The gene signature of the aortic mixed $CD4^+/CD8\alpha\beta^+$ T cell population showed the highest enrichment score with thymic $CD4^+CD8\alpha\beta^+$ cells, a progenitor stage of single $CD4^+$ and $CD8\alpha\beta^+$ $TCR\alpha\beta^+$ T cells (Fig1. B, Supplemental Table S1). To confirm extrathymic DPs with an independent method and assess whether DPs ($CD4^+CD8\alpha\beta^+$ $TCR\alpha\beta^-$) are also present in other organs or tissues, we performed a flow cytometry-based screening of 16 tissues of 8-week-old female wild-type *C57BL/6J* mice (Fig. S1). As expected, DPs represented the majority of leukocytes found in the thymus (Fig1. C). Only two other tissues contained DPs, (A) the mediastinal adipose tissue (MAT) connecting the thymus and the aortic arch (Mean ± SD: 9 % ± 12% of living leukocytes) and (B) aortic arches (Mean ± SD: 13% ± 11% of living leukocytes) (Fig. 1C). DPs were not detected in the abdominal aorta, which suggests their local confinement to the arch. Although the percentage of DPs among leukocytes found in the aortic arch was higher compared to the ones in MAT, absolute numbers were higher in MAT (Mean ± SD: 6765 ± 9448 vs. 315 ± 543 cells per mouse) (Fig. 1D). Of note, all DPs did not express surface CD3e (Fig. S2A). Few thymic DPs expressed CD69, a marker of positive selection, which was significantly reduced on MAT and aortic arch DPs (Fig. S2B). All three DP populations expressed TCRβ intracellularly, albeit at lower levels compared to lymph node CD4 T cells. The expression of intracellular TCR was significantly reduced in MAT and arch DPs compared to thymic DPs (Fig. S2C). To test whether the numbers of MAT and aortic arch DPs are specific for atherosclerosis-prone *C57BL/6J* mice, we also analyzed tissues from two-year old *BALB/C* mice, which are resistant to atherosclerosis (20). We found similar numbers in both strains (Fig. 1D). The abundance of aortic DPs was not altered in the course of atherosclerosis (Fig. S3). These findings point to homeostatic presence of these cells.

To address the location of extrathymic DPs, we performed 3D-whole mount imaging of cleared thymus with MAT and the aortic arch (Fig. 2A–C). DP cells were present in the MAT pads attached to the thymus capsule and in the adventitial space of the lower curvature of the aortic arch, where they were organized in clusters (Fig. 2B,C). Like thymic

DPs, extrathymic DPs were small, round cells, which was further established by sorting these cells directly onto glass slides followed by confocal microscopy (Fig. 2D, Fig. S4). Extrathymic DPs were slightly smaller compared to thymic DPs.

Extrathymic DPs have a distinct and region-specific transcriptional profile

To further establish if and how MAT and aortic arch DPs would differ from thymic DPs, we sorted DPs from all three regions by flow cytometry and subjected the cells to a low-input deep transcriptional profiling assay (10). Principal component analysis revealed the close relationship among DPs isolated from the same locations, as the transcriptomes of the individual biological replicates clustered closely together (Fig. 3a) However, the transcriptome of DPs differed in a location-specific and gradual manner in which thymic and aortic arch DPs represent the two ends of the spectrum bridged by MAT DPs. These results are also reflected in a heatmap comparing the collated transcriptomes (Fig. S5). (Fig. 3A,B, Fig. S5).

A total of 2147 genes were differentially regulated between the different DP populations (Fig. 3B, Supplemental Table S1). Extrathymic DPs had 858 genes upregulated and 1284 genes downregulated compared to thymic DPs. 94 genes were commonly regulated in the two extrathymic DP subsets (Fig. 3B, Supplemental Table S1), whereas 23 genes were uniquely expressed in MAT DPs. 31 different genes were exclusively expressed in aortic arch DPs.

Only expression of *Vps37b* increased in MAT in thymic DPs and was even higher expressed in aortic arch DPs compared to MAT DPs (Supplemental Table S1). VPS37B is a subunit of the ESCRT-I complex, which regulates vesicle trafficking and was recently identified by scRNA-seq of CD4 memory T cells residing in non-lymphoid tissue (21). *Hist3h2a* encodes for the histone H2A type 3. This gene is expressed higher by extrathymic DPs compared to thymic DPs, while its expression is higher in MAT DPs compared to aortic arch DPs. Virus-specific effector CD8$\alpha\beta^+$ T cells expressed higher *Hist3h2a* compared to virus-specific naïve T cells (22). MAT DPs also uniquely expressed *Rtel1*, whose protein product regulates telomere lengths. T cells deficient for *Rtel1* have reduced survival in long-term cultures (23). Several other genes were highly expressed among MAT DPs which are involved in regulating cell growth (*Slc25a10, Ftsj2, Ercc16*), apoptosis (*Sulf1, Dstyk*), or splicing (*Esrp2*). However, their functions in immune cells have yet to be determined.

Similarly, the top10 genes uniquely expressed in aortic arch DPs have unknown functions in T cells (*Abcd7, 1500004A13Rik, Metrnl, Gm12216, P4htm, Myl9, Rab44, E530011L22Rik*). Two genes were expressed in aortic arch DPs with known functions in T cells. The gene *Slc1a4* encodes for the alanine, serine, cysteine and threonine amino acid transporter ASCT1, which is strongly upregulated in activated T cells, providing sufficient metabolites for proliferation (24). The other gene was *Prf1* encoding for perforin 1, a well-known effector molecule of cytotoxic T cells. Perforin 1 is also expressed during positive selection of CD8 T cells and by thymocytes receiving MHC II-signals (25). Among the genes expressed by MAT and aortic arch DPs, but not thymic DPs, were a transcription factor (*Klf9*), signaling (*Fosl2, Gpr3, Lipt2*) and metabolism-relevant genes (*Dgat2, Klhl23*). Both cell populations also expressed *Hspa1a* encoding for the heat shock protein 72, which

is upregulated by cellular stress and has anti-inflammatory features (26). *Nr4a2* encodes for a member of the steroid-thyroid hormone-retinoid receptor superfamily. The deletion of this gene in $CD4^+$ T cells prevents Foxp3 expression and hence regulatory T cell (Treg) formation (27). *Rora* is expressed in Th17 cells, but the function in thymocytes is unknown. The transcription factor *Irf8* was described to facilitate TCR signal integration and differentiation of $CD8\alpha\beta^+$ T cells (28) and Th1-like Treg function (29), its function in DPs is, however, unknown. The gene *Il12rb2* encodes for the beta subunit of the interleukin 12 receptor complex. The cytokine IL-12 prevents thymic involution (30) and is important for differentiation of Th1, T_{FH1} (31) and TGF-beta induced Tregs (32). Extrathymic DPs also highly expressed *Slfn1*, a member of the Schlafen family. Ectopic *Slfn1* expression in thymocytes blocked DP development and caused cell cycle arrest by inhibiting cyclin D1 (33).

To test whether functional sets of genes were commonly up- or down-regulated between thymic and extrathymic DPs, we applied weighted correlation network analysis. A total of 33 gene modules were identified, of which 15 were significantly correlated with either thymic or extrathymic DPs (Fig. 3D). The most significant gene modules of the respective trait (thymic or extrathymic DP) contained also most genes. The turquoise gene module was the most significant module associating with the trait “thymic”. Pathway analysis demonstrated enrichment for signaling pathways involved in T cell development such as WNT signaling, TCR signaling, and Rap1 signaling (Fig. 3D), suggesting that thymic DPs are more mature in their developmental program. The most significant gene modules found in extrathymic DPs were enriched for cell cycle pathways and stress responses (Fig. 3D). Enrichment for cell cycle pathways suggests that these cells may recently have passed β-selection, advancing into the last proliferative burst during which their thymic counterparts would initiate CD4 and CD8 expression and TCRα-chain rearrangement. Although not among the differentially expressed genes between aortic arch DPs and thymic DPs, *pTa*, the gene encoding for the pre TCR alpha chain, was significantly lower expressed in MAT DPs compared aortic arch and thymic DPs (Supplemental Table S1). The appearance of stress response pathways might indicate the adaption of extrathymic DPs to the new and potentially non-favorable environment outside of the thymus.

Extrathymic and thymic DPs have a similar proliferative capacity and turn-over

The increased abundance of cell-cycle pathways among extrathymic DPs led us to investigate their proliferative capacity in more detail (Fig. 3D). *Mki67*, encoding for the proliferation marker Ki67, was equally highly expressed among DPs from all three tissues. On the protein level Ki67 was significantly higher expressed among MAT and aortic arch DPs, suggesting that these cells have a higher proliferative capacity (Fig. 4A). However, Ki67 marks actively proliferating cells and cells that just underwent a cell cycle, thus masking the cells that are currently undergoing proliferation. To further discriminate whether DPs from the three different locations exhibit altered proliferative capacity and turn-over, we performed a pulse-chase experiment by injecting EdU intraperitoneally into mice. EdU will be incorporated into the DNA of dividing cells and can be monitored by flow cytometry. One day after EdU injection, 20–30% of DPs across all three tissues incorporated EdU, pointing to similar proliferative capacity. The frequency of DPs that were positive for

EdU was reduced to 10% after three days, whilst no EdU-positive cells were detectable after five and seven days. DPs from all tissues followed the same pattern, indicating that the turn-over between thymic and extrathymic DP populations is similar (Fig. 4B).

Extrathymic DPs originate from the thymus

Developing T cells re-arrange the V, D, and J gene segments to form a functional TCR chain. This process is catalyzed by *Rag1* and *Rag2*. Transgenic $Rag2^{GFP}$ mice, which express green fluorescent protein (GFP) under the control of the *Rag2* promotor, demonstrated that GFP and *Rag2* was expressed at the late double-negative stage in the thymus. GFP expression decreased from the double negative stage to the single positive stage of thymic T cells, but remained detectable whilst *Rag2* expression disappears at the single-positive stage (34, 35). Interestingly, DPs from MAT and aortic arches displayed a significantly lower GFP signal than the two GFP expressing DP populations – called here GFP^{High} and GFP^{Low} – detected in the thymus. The reduced Rag2-GFP expression could be based on several mechanisms: Either extrathymic DPs have a constantly low RAG2-GFP expression or extrathymic DPs received a signal for TCR rearrangement before they had left the thymus (Fig. 5A). Bioinformatic TCR-alpha and TCR-beta chain repertoire analysis of thymic and extrathymic DPs revealed that TCR-alpha chain clonotypes were lower compared to beta chains in all three DP populations, whilst the ratio between both chains did not differ between DPs isolated from the three tissues (Fig. S6). This may suggest, that the beta-chain rearrangement has been finalized in all DPs and the alpha chain rearrangement has been initiated. The diversity of clonality defined by the Simpson Index is high and indicates a diverse TCR repertoire in all three DP populations. However, extrathymic DP development might have not further progressed past this stage as no rearranged surface TCR was detectable by flow cytometry (Fig. S1).

Rag2 expression is a prerequisite for T cell, B cell, and pre-TCR-expressing T cell progenitor presence in the thymus. To test whether *Rag2* is also necessary for extrathymic DP presence, we studied MAT and aortic arches of $Rag2^{-/-}$ mice. *Rag2* deficiency coincides with absence of MAT and aortic arch DPs (Fig. 5B). We further established the relationship of extrathymic with thymic DPs by thymectomizing 3-day and 21-day-old *C57BL/6J* mice. After a 6-week recovery period, we could not detect any MAT DPs by flow cytometry and the abundance of aortic arch DPs was drastically reduced (Fig. 5C).

Extrathymic DPs migrate locally

The drastically reduced presence of extrathymic DPs after thymectomy suggests that the thymus is the source of these cells. To further test this, we transplanted a third of a thymic lobe of a female, congenically-marked CD45.1 mouse under the kidney capsule of a female CD45.2 mice which were previously sham-operated or thymectomized. Presence of MAT and aortic arch DPs and their chimerism was assessed by flow cytometry 21 days post thymus transplantation (Fig. 6A). Thymectomy reduced the presence of DPs among living leukocytes in MAT (Sham (N=7) vs thymectomy (N=5): 10% ± 12% vs 0.05% ± 0.03% of living CD45) and aortic arch (Sham (N=6) vs thymectomy (N=5): 2.4% ± 3.1% vs 0.2% ± 0.1% of living $CD45^{+}$ cells). Transplantation of thymi under the kidney capsule did not lead to the accumulation of transplant-derived DPs in MAT or aortic arches (Fig. 6B) of

sham-operated mice. Similar results were obtained in thymectomized recipient mice. As a positive control, we confirmed accumulation of transplant-derived $CD4^+$ T cells in inguinal lymph nodes (Fig. S7). The failed population of transplant-derived DPs in MAT and aortic arches and their absence in the circulation (Fig. 1C) suggests that DPs do not enter the circulation. Thus, we hypothesized that extrathymic DPs migrate from the thymus and seed the MAT and aortic arch locally. To test this hypothesis, we blocked lymphocyte migration by pharmacologically inhibiting the sphingosine-1-phosphate receptor (S1P1) by injecting FTY720 every day for 7 days. As expected, the frequency of thymic DPs decreased while frequencies of thymic single $CD4^+$ T cells and $CD8^+$ T cells increased as they were trapped in the thymus (Fig. 6C–E). EdU injection demonstrated turn-over of all DPs within 5 days (Fig. 4C). Thus, if S1P1 was required for extrathymic DPs, we would expect reduced DP frequencies in MAT and aortic arches. However, neither MAT nor aortic arch abundance was altered, pointing to a locally confined mode of DP migration that does not require S1P1.

Extrathymic DPs differentiate into single positive T cells with a CD4 bias

To test whether extrathymic DPs are capable of developing into single $CD4^+$ and $CD8\alpha\beta^+$ T cells, we flow sorted DPs from MAT and aortic arches of female, 8-week-old *C57BL6/J* mice and subjected them to a hanging-drop fetal thymic organ culture (Fig. 7). Thymi were isolated from E14 *CD45.1/CD45.2* embryos. At day 10 of eight individual fetal thymic organ cultures, 20% of extrathymic $CD4^+CD8\alpha\beta^+$ CD45.2 cells expressed surface TCRβ. Half of these cells were expressing both CD4 and CD8, whereas the majority of single positive T cells were CD4 positive (Fig. 7). TCRβ-negative extrathymic DPs were mostly CD4 and CD8 double positive.

Next, we tested whether extrathymic DPs interacted with other cells in the tissue. Invariant natural killer T (iNKT) cells need interactions with thymic DPs for their development and differentiation (36). iNKT cells are present in adipose tissue and play a prominent role in adipose tissue inflammation (37), although the exact nature of this role is controversial. First, we tested whether MAT, like other adipose tissues, contains iNKT cells. Confocal imaging of whole mount mediastinal adipose tissue fat pads stained with a fluorochrome-conjugated CD1d-tetramer loaded with alpha-galactosylceramide (alpha-GalCer) showed the presence of iNKT cells (Fig. 8A). The detection threshold was determined by a sample stained with empty fluorochrome-conjugated CD1d-tetramer. In 10 independent regions of interest, we found 76 CD1d-$tetramer^+$ cells. We simultaneously stained for CD4 and CD8α in the staining and detected 37 $CD4^+CD8\alpha^+$ cells, indicating that iNKT cells outnumber DPs in MAT. Isosurface rendering revealed that DPs clustered around and in close proximity to iNKT cells (Fig. 8B–D). Quantification of ten independent regions of interest in MAT showed that the distance from DPs to iNKT cells was 23μm, whereas iNKT cells have a distance of 56μm to $CD4^+CD8\alpha^+$ cells (Fig. 8E). This supports the notion that $CD4^+CD8\alpha^+$ cells in MAT reside close to iNKT cells, whereas some iNKT cells are distant from DPs. We further confirmed expression of CD1d by extra-thymic DPs (Fig. S8). To test whether MAT DPs might interact with iNKT cells, we designed a glycolipid antigen restimulation experiment. In brief, DPs were isolated from MAT and as a control from the thymus of *C57BL/6J* mice and pulsed with alpha-GalCer. Varying numbers of MAT and thymic DPs were co-cultured with the DN3A4-1.2 hybridoma iNKT cell line for 12h (7). This cell

line specifically responds to antigenic stimulation by CD69 expression and IL-2 secretion. Due to limited DP numbers in MAT and aortic arches, we decided to co-culture 50k MAT DPs with 50k DN3A4-1.2 hybridoma iNKT cells. The co-culture of DPs from either origin with the hybridoma cells induced a similar expression of surface CD69 (Fig. 8F) on the iNKT cells and similar amount of IL-2 (Fig. 8G) secreted into the culture supernatant. Both responses were detectable over the included co-culture controls without alpha-GalCer, and there was no difference whether thymic or MAT DPs were used at 50k cells. This experiment demonstrates that MAT DPs can activate iNKT cells in vitro.

Discussion:

In the current study, we demonstrate the presence of DPs in MAT and aortic arches of wild-type mice. DP thymocytes are a heterogenous population. Blastic DPs are highly proliferative and do not express a surface TCR or CD3e, similar to extrathymic DPs. The process of β−selection induces a proliferative burst, dependent on c-Myc activity (38), pre-TCR (39) and Notch signaling (40). We show extrathymic DP proliferation by Ki67-staining and turn-over by a BrdU pulse experiment. Signaling via the pre-TCR suppresses Notch signaling dependent pathways which halts the proliferative burst of blastic DPs and starts their transition into quiescent small DPs (41). The shift from blastic DPs to small DPs was associated with a strong change in gene expression and downregulated many genes, 100 of which were involved in metabolism (41). Small DPs engage in positive selection to test their newly rearranged and surface expressed αβ-TCR for binding to self-peptides presented in MHC complexes (42). Like blastic thymic DPs, extrathymic lack surface expression of CD3e and TCRβ, but are considerably smaller. Successful rearrangement and signaling via the αβ-TCR upregulated surface expression of the activation marker CD69 on the small DPs, labeling these cells $CD69^{+}$ DPs (43). Extrathymic DPs do not express CD69 and they have lower $Rag2^{GFP}$ expression, which suggests that they are similar to blastic DPs in the thymus and are in a proliferative phase.

Deep transcriptional profiling revealed differences between DP cells isolated from the three locations. Thymic DPs were enriched for pathways involved in TCR signaling and extrathymic DPs demonstrated stress responses and elevated cell cycle pathways. Only 94 genes are significantly overexpressed by aortic arch and MAT DPs compared to thymic DPs. Both populations of extrathymic DPs expressed *Grn* encoding for granulin. Granulin is a secreted protein with numerous functions including tissue growth, wound healing and inflammation (44) and has been implicated in myelopoiesis (45). The cognate receptor is unknown, but granulin can bind many receptors including TNF receptors, Notch, Toll-like receptor 9, LDL Receptor Related Protein 1 (LRP1) and sortilin1 and induce their downstream signaling cascades (46). It is thus tempting to speculate that extrathymic DPs could contribute to local tissue homeostasis and wound repair. Although the three DP populations are transcriptomically different from each other, we would like to acknowledge that the current analysis is limited and the magnitude of this difference in comparison to other thymocyte populations is unknown.

Although both extrathymic DP populations express genes that are involved in the development and effector function of CD4 and CD8 T cell subsets (*Irf8* (28, 29), *Il12rb2*

(31, 32), neither DP population differentially expressed genes that would determine commitment to the CD4 (*Thpok* (47)) or CD8 (*Runx3* (48)) T cell lineage. Aortic arch DPs uniquely expressed *Prf1* encoding for perforin, which is expressed during positive selection of CD8 T cells and by thymocytes receiving MHC II-signals (25). We demonstrate that extrathymic DPs are capable of developing into single positive T cells in an *in vitro* hanging drop culture. The mediastinal adipose tissue isolated DP cells outnumbered the aortic arch DPs by 10:1 in our cell culture system, as determined by flow cytometry. Because of the low cell numbers, we were unable to test the aortic arch DPs in the hanging drop culture system.

Our data that extrathymic DP cells reside near iNKT cells and that DP cells express the MHC-like molecule CD1d suggest that they may be involved in activating iNKT cells. It should be noted that many cell types express CD1d and can activate iNKT cells (49). iNKT cells exist in different flavors and exert tissue-specific roles (50). They are prominent mediators of adipose tissue inflammation (37) or atherosclerosis (51), but also can protect from obesity through regulatory cytokine production (52). We provide evidence that MAT DPs can present lipid antigen and activate iNKT hybridoma cells *in vitro* and cluster around them *in vivo*. However, further research will have to clarify which antigens MAT DPs would present and if they indeed can activate a polyclonal iNKT response and how this would be shaped.

The occurrence of a cervical thymus is common in humans (53). The function of these structures is unknown, although they are considered to be origin sites of cervical thymomas in humans (54, 55). In 2006, Terszowski and colleagues reported presence of a cervical thymus in multiple mouse strains including C57BL/6J mice (56). This structure is however located at a different anatomical side in the neck in distance to the aortic arch or MAT. The close vicinity of the aortic arch and MAT to the thymus and the rather large distance to cervical thymi suggest that the DPs in these to extra-thymic tissues migrate locally from the thymus, which we further confirmed experimentally. The pharmacological inhibition of S1P1R trapped $CD4^+$ and $CD8^+$ T cells in the thymus as expected, but did not alter the presence of DP numbers in MAT and the aortic arch, suggesting that they do not enter the circulation and migrate locally. Transplantation of congenically marked thymi under the kidney capsule failed to reconstitute DPs in the mediastinal adipose tissue or aortic arch.

Recent studies employing mass cytometry, single cell RNA sequencing (scRNA-seq) or cellular indexing of transcriptomes and epitopes by sequencing (CITE-seq) to uncover cellular heterogeneity in human and mouse atherosclerosis identified the existence of aortic and plaque-resident $CD4^+CD8\alpha\beta^+$ T cells (3, 57, 58). In a recent meta-analysis integrating single cell transcriptomes from aortic leukocytes in atherosclerosis, we identified a cluster with mixed phenotype of single-positive *Cd4*$^+$ and *Cd8*$^+$ T cells (59). This cluster accounted for ~13–26% of aortic T cells in scRNA-seq, a frequency we also observed by flow cytometry in young and old wildtype mice in the present study. Although the frequency of DPs was higher in atherosclerotic mouse aortas as assayed by flow cytometry, their relative abundance did not change with disease progression. Thus, we have no evidence that aortic and MAT DPs are related to cardiovascular disease. Mass cytometric analysis of human atherosclerotic plaques also uncovered $CD4^+CD8\alpha\beta^+$ T cells. Unlike mouse DPs, these cells had relevant cell surface expression of CD3 (57). Indeed, mature human

$CD3^+CD4^+CD8\alpha\beta^+$ T cells have been identified in tumors (60, 61) and the circulation of patients with rheumatoid arthritis (62). These cells lacked expression of relevant thymocyte markers and are likely a mature independent subset different from the immature DP cells uncovered here.

Taken together, our findings define two new, transcriptionally distinct subsets of extrathymic DPs that escape from the thymus independent of S1P1.

Supplementary Material

Refer to Web version on PubMed Central for supplementary material.

Acknowledgments:

We would like to thank Cheryl Kim, Denise Hinz, Christopher Dillingham, and Matthew Haynes for cell sorting, Zbigniew Mikulski and Sara McArdle for expert help with imaging analysis. We would also like to thank Dr. Ellen Rothenberg for her kind advise and critical feedback throughout the preparation of the manuscript.

Grant support

The present work was supported by grants HL115232, HL88093, and HL121697 from the National Heart, Lung and Blood Institute to K.L. H.W. was supported by Deutsche Forschungsgemeinschaft (GZ WI 4811/1-1, and SFB TRR259 397484323) and the Tullie and Rickey Families SPARK Award for Innovations in Immunology. The FACSAriaII Cell Sorter, the Zeiss LSM 880, and Illumina HiSeq2500 were acquired through the Shared Instrumentation Grant Programs S10 RR027366, S10 OD021831, and S10 OD16262.

References:

1. Wolf D, and Ley K. 2019. Immunity and Inflammation in Atherosclerosis. Circ Res 124: 315–327. [PubMed: 30653442]
2. Winkels H, Ehinger E, Vassallo M, Buscher K, Dinh H, Kobiyama K, Hamers A, Cochain C, Vafadarnejad E, Saliba AE, Zernecke A, Pramod A, Ghosh A, Anto Michel N, Hoppe N, Hilgendorf I, Zirlik A, Hedrick C, Ley K, and Wolf D. 2018. Atlas of the Immune Cell Repertoire in Mouse Atherosclerosis Defined by Single-Cell RNA-Sequencing and Mass Cytometry. Circ Res.
3. Cochain C, Vafadarnejad E, Arampatzi P, Jaroslav P, Winkels H, Ley K, Wolf D, Saliba AE, and Zernecke A. 2018. Single-Cell RNA-Seq Reveals the Transcriptional Landscape and Heterogeneity of Aortic Macrophages in Murine Atherosclerosis. Circ Res.
4. Hosokawa H, and Rothenberg EV. 2018. Cytokines, Transcription Factors, and the Initiation of T-Cell Development. Cold Spring Harb Perspect Biol 10.
5. Galkina E, Kadl A, Sanders J, Varughese D, Sarembock IJ, and Ley K. 2006. Lymphocyte recruitment into the aortic wall before and during development of atherosclerosis is partially L-selectin dependent. J Exp Med 203: 1273–1282. [PubMed: 16682495]
6. Li W, Germain RN, and Gerner MY. 2017. Multiplex, quantitative cellular analysis in large tissue volumes with clearing-enhanced 3D microscopy (Ce3D). Proc Natl Acad Sci U S A 114: E7321–E7330. [PubMed: 28808033]
7. Burdin N, Brossay L, Koezuka Y, Smiley ST, Grusby MJ, Gui M, Taniguchi M, Hayakawa K, and Kronenberg M. 1998. Selective ability of mouse CD1 to present glycolipids: alpha-galactosylceramide specifically stimulates V alpha 14+ NK T lymphocytes. J Immunol 161: 3271–3281. [PubMed: 9759842]
8. Subramanian A, Tamayo P, Mootha VK, Mukherjee S, Ebert BL, Gillette MA, Paulovich A, Pomeroy SL, Golub TR, Lander ES, and Mesirov JP. 2005. Gene set enrichment analysis: a knowledge-based approach for interpreting genome-wide expression profiles. Proc Natl Acad Sci U S A 102: 15545–15550. [PubMed: 16199517]

9. Barbie DA, Tamayo P, Boehm JS, Kim SY, Moody SE, Dunn IF, Schinzel AC, Sandy P, Meylan E, Scholl C, Frohling S, Chan EM, Sos ML, Michel K, Mermel C, Silver SJ, Weir BA, Reiling JH, Sheng Q, Gupta PB, Wadlow RC, Le H, Hoersch S, Wittner BS, Ramaswamy S, Livingston DM, Sabatini DM, Meyerson M, Thomas RK, Lander ES, Mesirov JP, Root DE, Gilliland DG, Jacks T, and Hahn WC. 2009. Systematic RNA interference reveals that oncogenic KRAS-driven cancers require TBK1. Nature 462: 108–112. [PubMed: 19847166]
10. Rosales SL, Liang S, Engel I, Schmiedel BJ, Kronenberg M, Vijayanand P, and Seumois G. 2018. A Sensitive and Integrated Approach to Profile Messenger RNA from Samples with Low Cell Numbers. Methods Mol Biol 1799: 275–302. [PubMed: 29956159]
11. Andrews S 2010. FastQC: A Quality Control Tool for High Throughput Sequence Data [Online]. Available online at: http://www.bioinformatics.babraham.ac.uk/projects/fastqc/.
12. Dobin A, Davis CA, Schlesinger F, Drenkow J, Zaleski C, Jha S, Batut P, Chaisson M, and Gingeras TR. 2013. STAR: ultrafast universal RNA-seq aligner. Bioinformatics 29: 15–21. [PubMed: 23104886]
13. Yates AD, Achuthan P, Akanni W, Allen J, Allen J, Alvarez-Jarreta J, Amode MR, Armean IM, Azov AG, Bennett R, Bhai J, Billis K, Boddu S, Marugan JC, Cummins C, Davidson C, Dodiya K, Fatima R, Gall A, Giron CG, Gil L, Grego T, Haggerty L, Haskell E, Hourlier T, Izuogu OG, Janacek SH, Juettemann T, Kay M, Lavidas I, Le T, Lemos D, Martinez JG, Maurel T, McDowall M, McMahon A, Mohanan S, Moore B, Nuhn M, Oheh DN, Parker A, Parton A, Patricio M, Sakthivel MP, Abdul Salam AI, Schmitt BM, Schuilenburg H, Sheppard D, Sycheva M, Szuba M, Taylor K, Thormann A, Threadgold G, Vullo A, Walts B, Winterbottom A, Zadissa A, Chakiachvili M, Flint B, Frankish A, Hunt SE, G II, Kostadima M, Langridge N, Loveland JE, Martin FJ, Morales J, Mudge JM, Muffato M, Perry E, Ruffier M, Trevanion SJ, Cunningham F, Howe KL, Zerbino DR, and Flicek P. 2020. Ensembl 2020. Nucleic Acids Res 48: D682–D688. [PubMed: 31691826]
14. Hartley SW, and Mullikin JC. 2015. QoRTs: a comprehensive toolset for quality control and data processing of RNA-Seq experiments. BMC Bioinformatics 16: 224. [PubMed: 26187896]
15. Tange O 2011. GNU Parallel - The Command-Line Power Tool. The USENIX Magazine 36: 42–47.
16. Love MI, Huber W, and Anders S. 2014. Moderated estimation of fold change and dispersion for RNA-seq data with DESeq2. Genome Biol 15: 550. [PubMed: 25516281]
17. Lex A, Gehlenborg N, Strobelt H, Vuillemot R, and Pfister H. 2014. UpSet: Visualization of Intersecting Sets. IEEE Trans Vis Comput Graph 20: 1983–1992. [PubMed: 26356912]
18. Langfelder P, and Horvath S. 2008. WGCNA: an R package for weighted correlation network analysis. BMC Bioinformatics 9: 559. [PubMed: 19114008]
19. Bolotin DA, Poslavsky S, Davydov AN, Frenkel FE, Fanchi L, Zolotareva OI, Hemmers S, Putintseva EV, Obraztsova AS, Shugay M, Ataullakhanov RI, Rudensky AY, Schumacher TN, and Chudakov DM. 2017. Antigen receptor repertoire profiling from RNA-seq data. Nat Biotechnol 35: 908–911. [PubMed: 29020005]
20. Lusis AJ, Seldin MM, Allayee H, Bennett BJ, Civelek M, Davis RC, Eskin E, Farber CR, Hui S, Mehrabian M, Norheim F, Pan C, Parks B, Rau CD, Smith DJ, Vallim T, Wang Y, and Wang J. 2016. The Hybrid Mouse Diversity Panel: a resource for systems genetics analyses of metabolic and cardiovascular traits. J Lipid Res 57: 925–942. [PubMed: 27099397]
21. Miragaia RJ, Gomes T, Chomka A, Jardine L, Riedel A, Hegazy AN, Whibley N, Tucci A, Chen X, Lindeman I, Emerton G, Krausgruber T, Shields J, Haniffa M, Powrie F, and Teichmann SA. 2019. Single-Cell Transcriptomics of Regulatory T Cells Reveals Trajectories of Tissue Adaptation. Immunity 50: 493–504 e497. [PubMed: 30737144]
22. Wherry EJ, Ha SJ, Kaech SM, Haining WN, Sarkar S, Kalia V, Subramaniam S, Blattman JN, Barber DL, and Ahmed R. 2007. Molecular signature of CD8+ T cell exhaustion during chronic viral infection. Immunity 27: 670–684. [PubMed: 17950003]
23. Speckmann C, Sahoo SS, Rizzi M, Hirabayashi S, Karow A, Serwas NK, Hoemberg M, Damatova N, Schindler D, Vannier JB, Boulton SJ, Pannicke U, Gohring G, Thomay K, Verdu-Amoros JJ, Hauch H, Woessmann W, Escherich G, Laack E, Rindle L, Seidl M, Rensing-Ehl A, Lausch E, Jandrasits C, Strahm B, Schwarz K, Ehl SR, Niemeyer C, Boztug K, and Wlodarski MW. 2017.

Corrigendum: Clinical and Molecular Heterogeneity of RTEL1 Deficiency. Front Immunol 8: 1250. [PubMed: 28989339]

24. Levring TB, Hansen AK, Nielsen BL, Kongsbak M, von Essen MR, Woetmann A, Odum N, Bonefeld CM, and Geisler C. 2012. Activated human CD4+ T cells express transporters for both cysteine and cystine. Sci Rep 2: 266. [PubMed: 22355778]
25. Liu X, Taylor BJ, Sun G, and Bosselut R. 2005. Analyzing expression of perforin, Runx3, and Thpok genes during positive selection reveals activation of CD8-differentiation programs by MHC II-signaled thymocytes. J Immunol 175: 4465–4474. [PubMed: 16177089]
26. Borges TJ, Wieten L, van Herwijnen MJ, Broere F, van der Zee R, Bonorino C, and van Eden W. 2012. The anti-inflammatory mechanisms of Hsp70. Front Immunol 3: 95. [PubMed: 22566973]
27. Sekiya T, Kashiwagi I, Inoue N, Morita R, Hori S, Waldmann H, Rudensky AY, Ichinose H, Metzger D, Chambon P, and Yoshimura A. 2011. The nuclear orphan receptor Nr4a2 induces Foxp3 and regulates differentiation of CD4+ T cells. Nat Commun 2: 269. [PubMed: 21468021]
28. Miyagawa F, Zhang H, Terunuma A, Ozato K, Tagaya Y, and Katz SI. 2012. Interferon regulatory factor 8 integrates T-cell receptor and cytokine-signaling pathways and drives effector differentiation of CD8 T cells. Proc Natl Acad Sci U S A 109: 12123–12128. [PubMed: 22783014]
29. Lee W, Kim HS, Baek SY, and Lee GR. 2016. Transcription factor IRF8 controls Th1-like regulatory T-cell function. Cell Mol Immunol 13: 785–794. [PubMed: 26166768]
30. Li L, Hsu HC, Stockard CR, Yang P, Zhou J, Wu Q, Grizzle WE, and Mountz JD. 2004. IL-12 inhibits thymic involution by enhancing IL-7- and IL-2-induced thymocyte proliferation. J Immunol 172: 2909–2916. [PubMed: 14978093]
31. Powell MD, Read KA, Sreekumar BK, Jones DM, and Oestreich KJ. 2019. IL-12 signaling drives the differentiation and function of a TH1-derived TFH1-like cell population. Sci Rep 9: 13991. [PubMed: 31570752]
32. Zhao Z, Yu S, Fitzgerald DC, Elbehi M, Ciric B, Rostami AM, and Zhang GX. 2008. IL-12R beta 2 promotes the development of CD4+CD25+ regulatory T cells. J Immunol 181: 3870–3876. [PubMed: 18768841]
33. Schwarz DA, Katayama CD, and Hedrick SM. 1998. Schlafen, a new family of growth regulatory genes that affect thymocyte development. Immunity 9: 657–668. [PubMed: 9846487]
34. Boursalian TE, Golob J, Soper DM, Cooper CJ, and Fink PJ. 2004. Continued maturation of thymic emigrants in the periphery. Nat Immunol 5: 418–425. [PubMed: 14991052]
35. Yu W, Nagaoka H, Jankovic M, Misulovin Z, Suh H, Rolink A, Melchers F, Meffre E, and Nussenzweig MC. 1999. Continued RAG expression in late stages of B cell development and no apparent re-induction after immunization. Nature 400: 682–687. [PubMed: 10458165]
36. Hogquist K, and Georgiev H. 2020. Recent advances in iNKT cell development. F1000Res 9.
37. Park YJ, Park J, Huh JY, Hwang I, Choe SS, and Kim JB. 2018. Regulatory Roles of Invariant Natural Killer T Cells in Adipose Tissue Inflammation: Defenders Against Obesity-Induced Metabolic Complications. Front Immunol 9: 1311. [PubMed: 29951059]
38. Dose M, Khan I, Guo Z, Kovalovsky D, Krueger A, von Boehmer H, Khazaie K, and Gounari F. 2006. c-Myc mediates pre-TCR-induced proliferation but not developmental progression. Blood 108: 2669–2677. [PubMed: 16788099]
39. Ciofani M, Schmitt TM, Ciofani A, Michie AM, Cuburu N, Aublin A, Maryanski JL, and Zuniga-Pflucker JC. 2004. Obligatory role for cooperative signaling by pre-TCR and Notch during thymocyte differentiation. J Immunol 172: 5230–5239. [PubMed: 15100261]
40. Maillard I, Tu L, Sambandam A, Yashiro-Ohtani Y, Millholland J, Keeshan K, Shestova O, Xu L, Bhandoola A, and Pear WS. 2006. The requirement for Notch signaling at the beta-selection checkpoint in vivo is absolute and independent of the pre-T cell receptor. J Exp Med 203: 2239–2245. [PubMed: 16966428]
41. Mingueneau M, Kreslavsky T, Gray D, Heng T, Cruse R, Ericson J, Bendall S, Spitzer MH, Nolan GP, Kobayashi K, von Boehmer H, Mathis D, Benoist C, Immunological Genome C, Best AJ, Knell J, Goldrath A, Joic V, Koller D, Shay T, Regev A, Cohen N, Brennan P, Brenner M, Kim F, Nageswara Rao T, Wagers A, Heng T, Ericson J, Rothamel K, Ortiz-Lopez A, Mathis D, Benoist C, Bezman NA, Sun JC, Min-Oo G, Kim CC, Lanier LL, Miller J, Brown B, Merad M, Gautier EL, Jakubzick C, Randolph GJ, Monach P, Blair DA, Dustin ML, Shinton SA, Hardy RR, Laidlaw

D, Collins J, Gazit R, Rossi DJ, Malhotra N, Sylvia K, Kang J, Kreslavsky T, Fletcher A, Elpek K, Bellemare-Pelletier A, Malhotra D, and Turley S. 2013. The transcriptional landscape of alphabeta T cell differentiation. Nat Immunol 14: 619–632. [PubMed: 23644507]

42. Starr TK, Jameson SC, and Hogquist KA. 2003. Positive and negative selection of T cells. Annu Rev Immunol 21: 139–176. [PubMed: 12414722]
43. Swat W, Dessing M, von Boehmer H, and Kisielow P. 1993. CD69 expression during selection and maturation of CD4+8+ thymocytes. Eur J Immunol 23: 739–746. [PubMed: 8095460]
44. Bateman A, Cheung ST, and Bennett HPJ. 2018. A Brief Overview of Progranulin in Health and Disease. Methods Mol Biol 1806: 3–15. [PubMed: 29956265]
45. Campbell C, Fursova O, Cheng X, Snella E, McCune A, Li L, Solchenberger B, Schmid B, Morton SD,M, Traver D, and Espin-Palazon R. 2020. A zebrafish model of Granulin deficiency reveals essential roles in myeloid cell differentiation. bioRxiv 10.1101/2020.07.23.217067.
46. Chitramuthu BP, Bennett HPJ, and Bateman A. 2017. Progranulin: a new avenue towards the understanding and treatment of neurodegenerative disease. Brain 140: 3081–3104. [PubMed: 29053785]
47. He X, He X, Dave VP, Zhang Y, Hua X, Nicolas E, Xu W, Roe BA, and Kappes DJ. 2005. The zinc finger transcription factor Th-POK regulates CD4 versus CD8 T-cell lineage commitment. Nature 433: 826–833. [PubMed: 15729333]
48. Woolf E, Xiao C, Fainaru O, Lotem J, Rosen D, Negreanu V, Bernstein Y, Goldenberg D, Brenner O, Berke G, Levanon D, and Groner Y. 2003. Runx3 and Runx1 are required for CD8 T cell development during thymopoiesis. Proc Natl Acad Sci U S A 100: 7731–7736. [PubMed: 12796513]
49. Brigl M, and Brenner MB. 2004. CD1: antigen presentation and T cell function. Annu Rev Immunol 22: 817–890. [PubMed: 15032598]
50. Crosby CM, and Kronenberg M. 2018. Tissue-specific functions of invariant natural killer T cells. Nat Rev Immunol 18: 559–574. [PubMed: 29967365]
51. Getz GS, and Reardon CA. 2017. Natural killer T cells in atherosclerosis. Nat Rev Cardiol 14: 304–314. [PubMed: 28127028]
52. Lynch L, Nowak M, Varghese B, Clark J, Hogan AE, Toxavidis V, Balk SP, O'Shea D, O'Farrelly C, and Exley MA. 2012. Adipose tissue invariant NKT cells protect against diet-induced obesity and metabolic disorder through regulatory cytokine production. Immunity 37: 574–587. [PubMed: 22981538]
53. Prabhu AV, Kale HA, and Branstetter B. F. t.. 2015. Residual Cervical Thymus: A Normal CT Finding That May Be Present Throughout Patients' Lives. AJNR Am J Neuroradiol 36: 1525–1528. [PubMed: 25882283]
54. Tovi F, and Mares AJ. 1978. The aberrant cervical thymus. Embryology, Pathology, and clinical implications. Am J Surg 136: 631–637. [PubMed: 707745]
55. Yamashita H, Murakami N, Noguchi S, Noguchi A, Yokoyama S, Moriuchi A, and Nakayama I. 1983. Cervical thymoma and incidence of cervical thymus. Acta Pathol Jpn 33: 189–194. [PubMed: 6687653]
56. Terszowski G, Muller SM, Bleul CC, Blum C, Schirmbeck R, Reimann J, Pasquier LD, Amagai T, Boehm T, and Rodewald HR. 2006. Evidence for a functional second thymus in mice. Science 312: 284–287. [PubMed: 16513945]
57. Fernandez DM, Rahman AH, Fernandez NF, Chudnovskiy A, Amir ED, Amadori L, Khan NS, Wong CK, Shamailova R, Hill CA, Wang Z, Remark R, Li JR, Pina C, Faries C, Awad AJ, Moss N, Bjorkegren JLM, Kim-Schulze S, Gnjatic S, Ma'ayan A, Mocco J, Faries P, Merad M, and Giannarelli C. 2019. Single-cell immune landscape of human atherosclerotic plaques. Nat Med 25: 1576–1588. [PubMed: 31591603]
58. Winkels H, Ehinger E, Vassallo M, Buscher K, Dinh HQ, Kobiyama K, Hamers AAJ, Cochain C, Vafadarnejad E, Saliba AE, Zernecke A, Pramod AB, Ghosh AK, Anto Michel N, Hoppe N, Hilgendorf I, Zirlik A, Hedrick CC, Ley K, and Wolf D. 2018. Atlas of the Immune Cell Repertoire in Mouse Atherosclerosis Defined by Single-Cell RNA-Sequencing and Mass Cytometry. Circ Res 122: 1675–1688. [PubMed: 29545366]

59. Zernecke A, H. W, Cochain C, Williams J, Wolf D, Soehnlein O, Robbins C, Monaco M, Park I, McNamara C, Binder C, Cybulsky M, Scipione C, Hedrick C, Galkina E, Kyaw T, Ghosheh Y, Dinh H, Ley K. 2020. Meta-Analysis of Leukocyte Diversity in Atherosclerotic Mouse Aortas. Circulation Research, in press.

60. Overgaard NH, Jung JW, Steptoe RJ, and Wells JW. 2015. CD4+/CD8+ double-positive T cells: more than just a developmental stage? J Leukoc Biol 97: 31–38. [PubMed: 25360000]

61. Bohner P, Chevalier MF, Cesson V, Rodrigues-Dias SC, Dartiguenave F, Burruni R, Tawadros T, Valerio M, Lucca I, Nardelli-Haefliger D, Jichlinski P, and Derre L. 2019. Double Positive CD4(+)CD8(+) T Cells Are Enriched in Urological Cancers and Favor T Helper-2 Polarization. Front Immunol 10: 622. [PubMed: 30984190]

62. Quandt D, Rothe K, Scholz R, Baerwald CW, and Wagner U. 2014. Peripheral CD4CD8 double positive T cells with a distinct helper cytokine profile are increased in rheumatoid arthritis. PLoS One 9: e93293. [PubMed: 24667579]

Key points

- DPs reside in the mediastinal adipose tissue and aortic arch.
- Extrathymic DP presence depends on the thymus and RAG2 expression.
- Extrathymic DPs migrate locally.

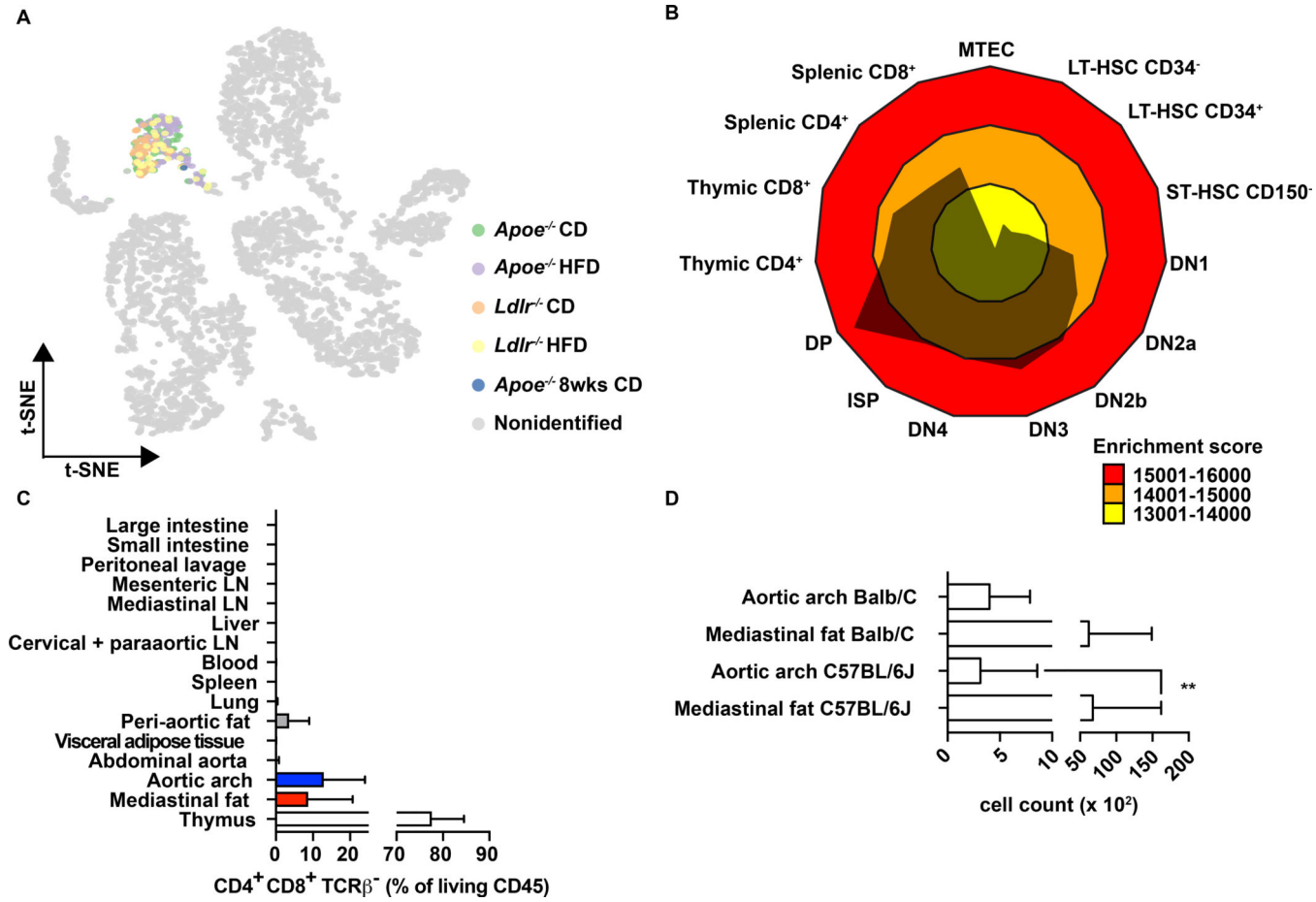

Figure 1. A new class of aortic immune cells

(**A**) Integrated single cell RNA sequencing analysis of living leukocytes isolated from atherosclerotic and non-atherosclerotic mice. (GSM2882367: 8-week-old male, *Ldlr*$^{-/-}$ mice fed 11 weeks western-type diet [yellow]; GSM2882368: 8-week-old male *Ldlr*$^{-/-}$ mice fed chow diet for 11 weeks [orange]; 8-week-old male *Apoe*$^{-/-}$ mice fed chow diet [blue]; 8-week-old male *Apoe*$^{-/-}$ mice fed chow diet for 12 weeks [green]; 8-week-old male *Apoe*$^{-/-}$ mice fed western-type diet for 12 weeks [purple]). All cells of the new immune cell subset cluster together and are found across all analyzed single cell RNA sequencing data sets as indicated by the different colors. All other aortic immune cell subsets were colored in grey. (**B**) The top 100 genes of the highlighted cluster in (**A**) were used for single sample gene set enrichment analysis of immune cell transcriptomes (GSE109125) isolated from bone marrow, spleen, and thymus. The enrichment score is displayed as spider plot. (**C**) Flow cytometric analysis of mentioned tissues for the presence of CD4^{+}CD8α^{+}TCR^{-} cells in 8-week-old, female *C57BL/6J* mice. For thymus N=49, mediastinal adipose tissue N=52, aortic arch N= 45 and all other tissues N=5. (**D**) Absolute numbers of CD4^{+}CD8α^{+}TCR^{-} cells in mediastinal adipose tissue (N=28) and aortic arches (N=29) of 8-week-old, female *C57BL/6J* mice and 2-year-old female *BALB/C* mice (N=4/tissue). (**C, D**) Data are presented as mean ± SD.

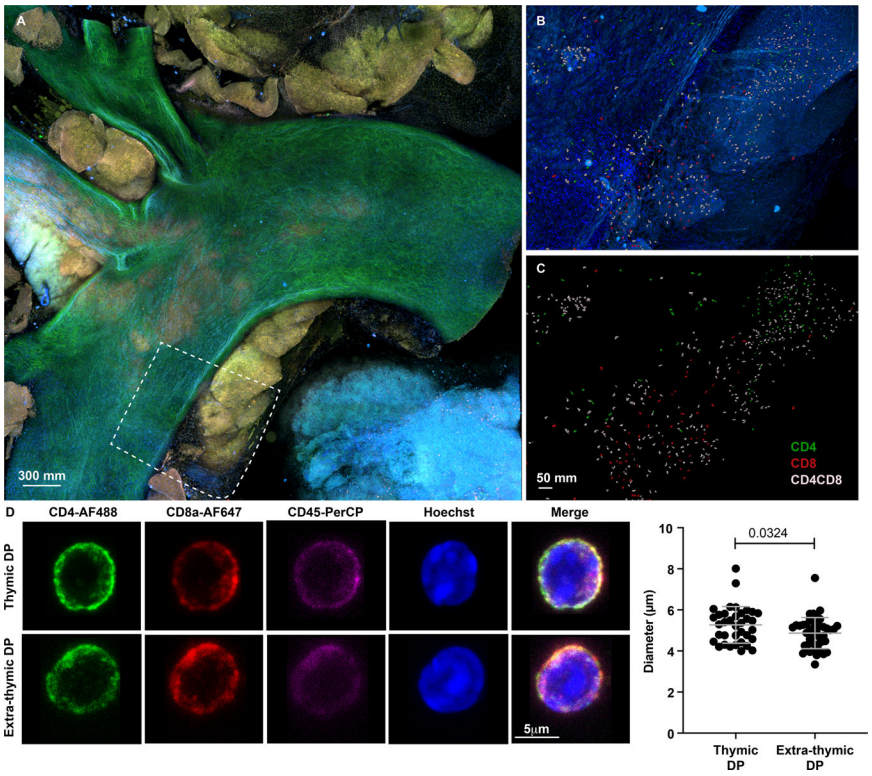

Figure 2. CD4CD8 cells are organized in clusters in the aortic arch

(**A**) Whole mount thymus, mediastinal adipose tissue, and aortic arch tissue of an 8-week-old, female *C57BL/6J* mouse was cleared according to the C_e3D protocol. The tissue preparation was stained for CD4 (green), CD8α (red), CD31 (pink), Nuclei, (Hoechst) and imaged by confocal microscopy. (**B**) Magnified region outlined by the dashed box in (**A**). (**C**) Spherical cells within the magnified area (**B**) were rendered by isosurfaces constructed in IMARIS. Isosurfaces of $CD4^+$ were colored in green, $CD8\alpha^+$ positive cells in red, and double positive cells are colored in white. The vasculature and nuclei are displayed in different shades of blue. Representative of three independent experiments. (**D**) Thymic and extrathymic $CD4^+CD8\alpha^+TCR^-$ cells of 8-week-old, female *C57BL/6J* mice (N=10) were sorted by flow cytometry onto a Poly-L-Lysine-coated glass slide and imaged by confocal microscopy. The distribution of the diameter is displayed.

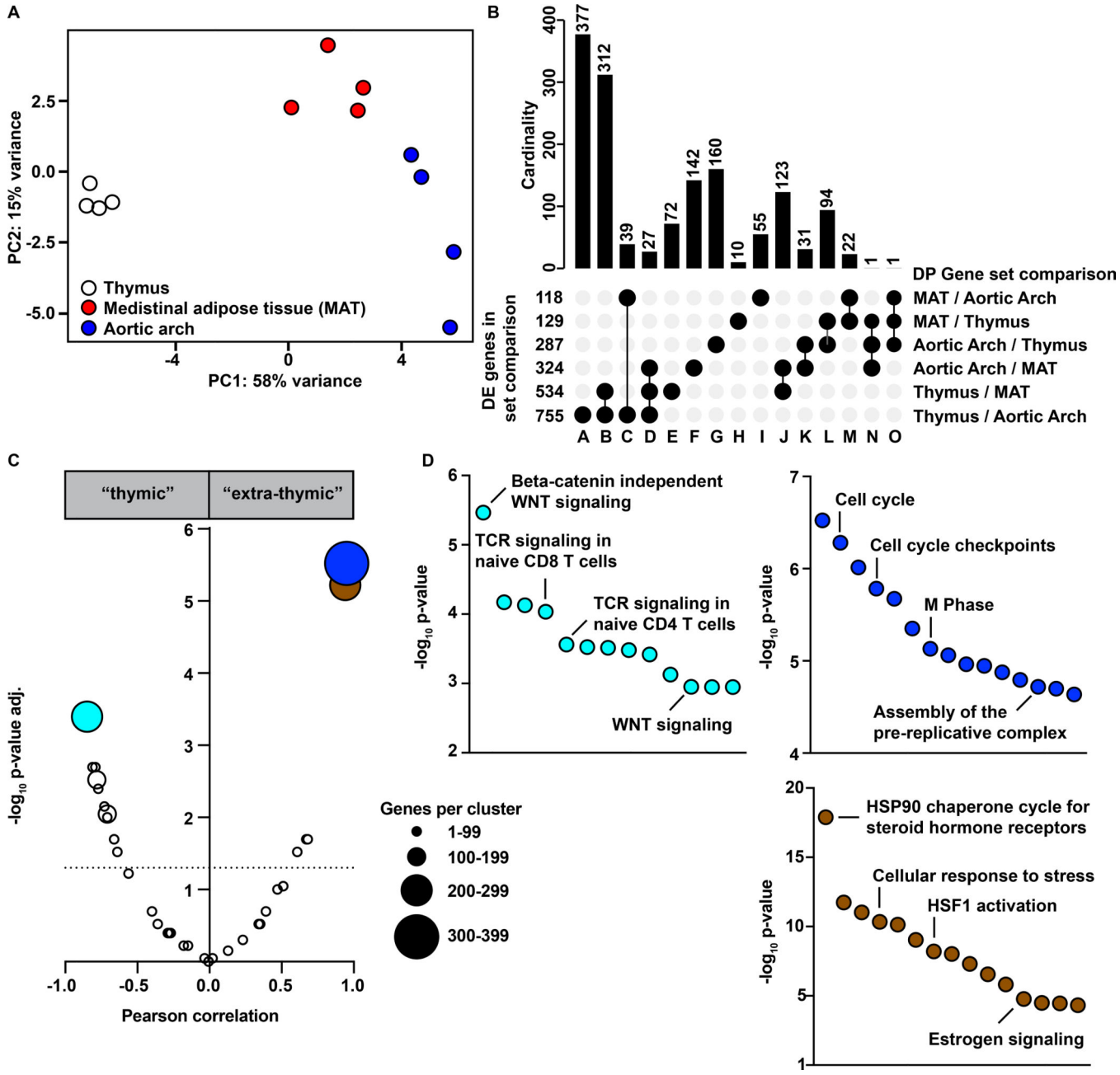

Figure 3. Extrathymic DPs differ transcriptomically from thymic DPs

(**A**) Living CD4^{+}CD8α^{+}TCR^{-} (DP) cells were isolated by FACS from thymus (white circles), mediastinal adipose tissue (red circles), and aortic arches (blue circles) of 8-week-old, female *C57BL/6J* mice (N=4). A low input SMART-Seq2 protocol was performed on multiple technical replicates (2–3/tissue) containing 200 cells each. The highly variable genes were obtained by principal component analysis. (**B**) UpSet analysis of differentially expressed genes of all possible comparisons between CD4^{+}CD8α^{+}TCR^{-} transcriptomes from the three tissues. Only differentially expressed genes with a log2-fold change above 2 or below −2 and an adjusted p-value <0.05 were considered. (**C**) Weighted correlation network analysis (WGCNA) resulting in 15 differentially regulated gene networks between

thymic, mediastinal adipose tissue, and aortic arch $CD4^{+}CD8\alpha^{+}TCR^{-}$ cells. The size of the dot represents the number of genes within the cluster. (**D**) The most significant gene networks of the top three correlating clusters (turquoise, blue, brown) were subjected to ConsensusPathDB (CPDB) pathway analysis and displayed with their respective p-values.

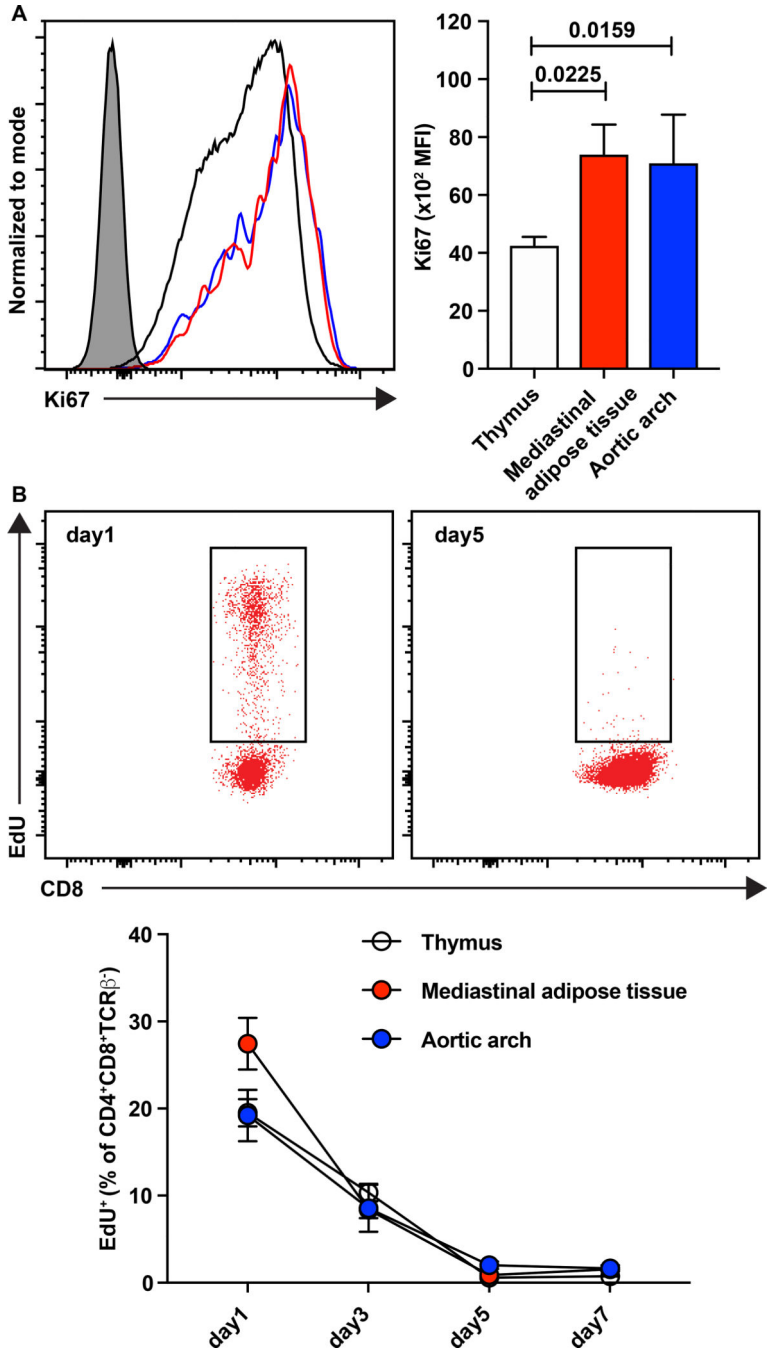

Figure 4. Extrathymic DPs are highly proliferative and have a fast turnover

(**A**) Quantification of the proliferation marker Ki67 among $CD4^{+}CD8\alpha^{+}TCR^{-}$ cells (DPs) from thymi (white bars and circles), mediastinal adipose tissue (red bars and circles), and aortic arches (blue bars and circles) of 8-week-old, female *C57BL/6J* mice (N=5). Representative histograms are displayed on the left and the mean fluorescence intensity is quantified on the right. (**B**) The base analogue EdU was injected intraperitoneally into 8-week-old, female *C57BL/6J* mice (1 mg/mouse) and DPs from thymus, mediastinal adipose tissue, and aortic arch were analyzed for EdU incorporation by flow cytometry day 1,

3, 5, and 7 post administration (N=5/timepoint). Representative flow cytometry plots are displayed on the top part and presence of EdU-positive DPs is quantified below.

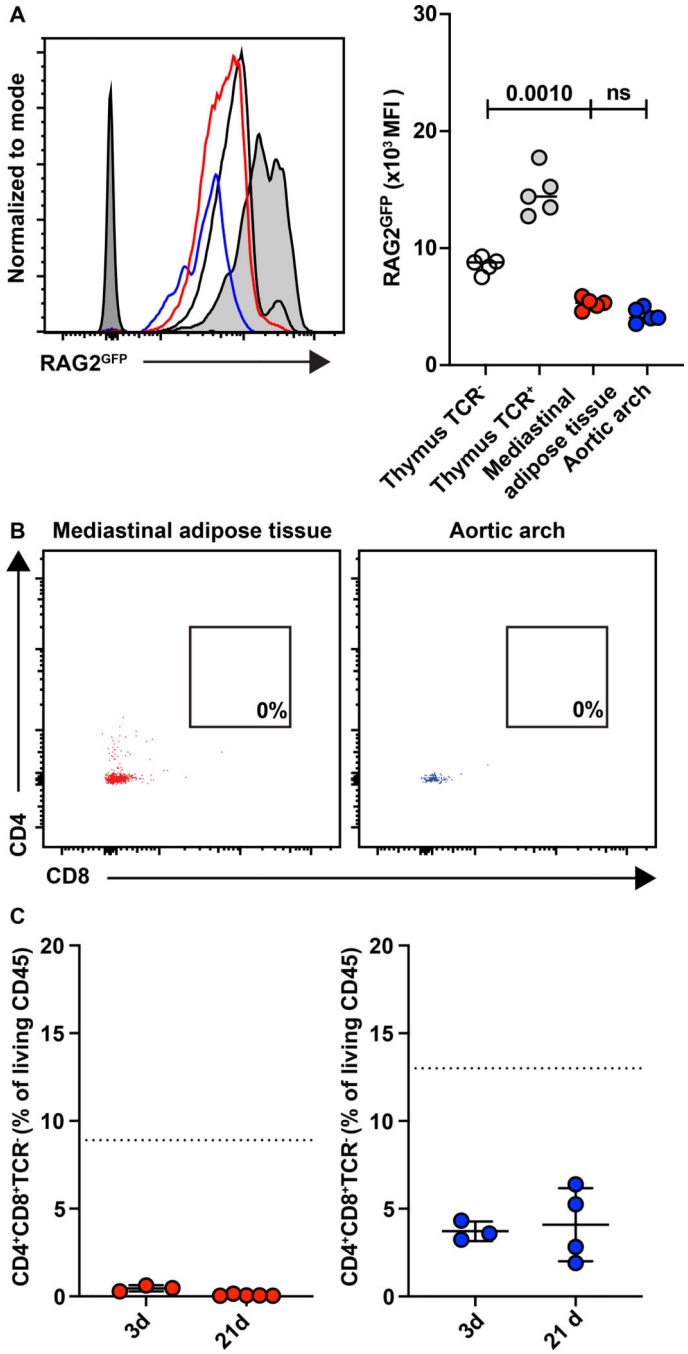

Figure 5. Extrathymic DP presence is thymus dependent

(**A**) $CD4^+CD8\alpha^+TCR\beta^-$ cells DPs from thymi (white circles, solid black line), mediastinal adipose tissue, (red circles, red line) and aortic arches (blue circles, blue line) and $CD4^+CD8\alpha^+TCR\beta^+$ cells in the thymus (grey circles, grey shaded line) were analyzed for RAG2 expression utilizing 8-week-old, female *Rag2*^{GFP} mice. Representative histograms are displayed on the left and the mean fluorescence intensity is quantified on the right. The dark grey line in the histogram indicates GFP background fluorescence in a *C57BL/6J* mouse. (**B**) Mediastinal adipose tissue and aortic arches of 8-week-old, female *Rag2*$^{-/-}$

mice were analyzed for presence of DPs by flow cytometry. Representative flow cytometry plots of three independent experiments are displayed. (**C**) Female *C57BL/6J* mice were thymectomized 3 days (N=3) and 21 days after birth (N=4). After a 6-week recovery period, mediastinal adipose tissue, and aortic arches were analyzed for presence of DPs by flow cytometry. Dotted lines: levels in intact mice (not thymectomized).

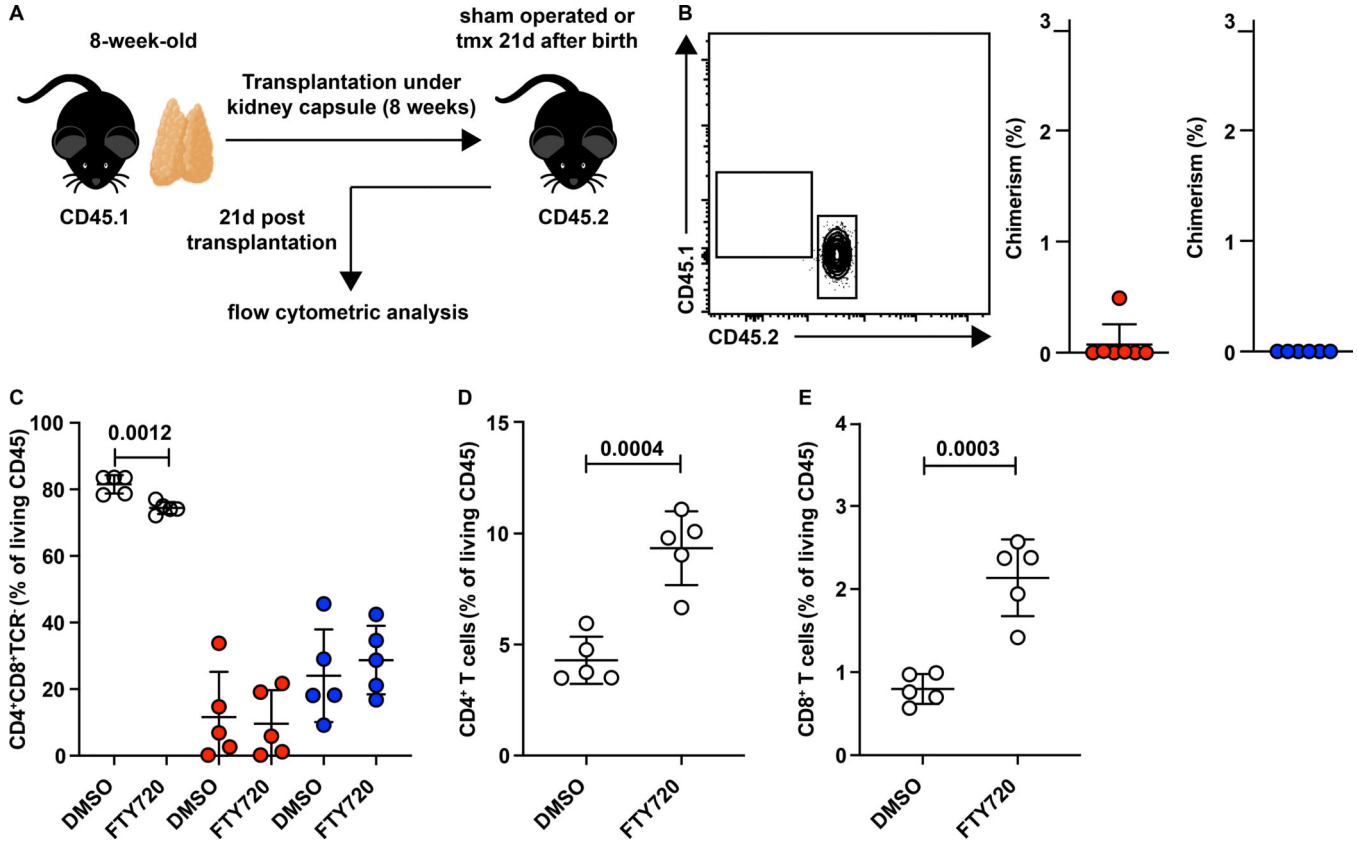

Figure 6. Extrathymic DP migration is locally restrained

(**A**) Experimental layout. 3-week-old, female *C57BL/6J* mice were thymectomized or sham operated. At the age of 8 weeks, mice transplanted with one third of a thymic lobe of a same-age, female *CD45.1 C57BL/6J* mice under the kidney capsule. Mice were sacrificed 21 days post transplantation and mediastinal adipose tissue and aortic arches were assessed for presence of DPs. (**B**) Representative flow cytometry plot of DPs in mediastinal adipose tissue of sham operated mice. The percent of chimerism in mediastinal adipose tissue (red dots) and aortic arch (blue dots) was quantified on the right. (**C**-**E**) 8-week-old, female *C57BL/6J* mice were injected intraperitoneally with DMSO alone or with 1mg/kg FTY720 in DMSO daily for 7 days (N=5/group). (**C**) Thymus, mediastinal adipose tissue, and aortic arch were analyzed for presence of DPs by flow cytometry. Thymic $CD4^+$ T cell content (**D**) and $CD8^+$ content (**E**) in DMSO and FTY720-treated mice.

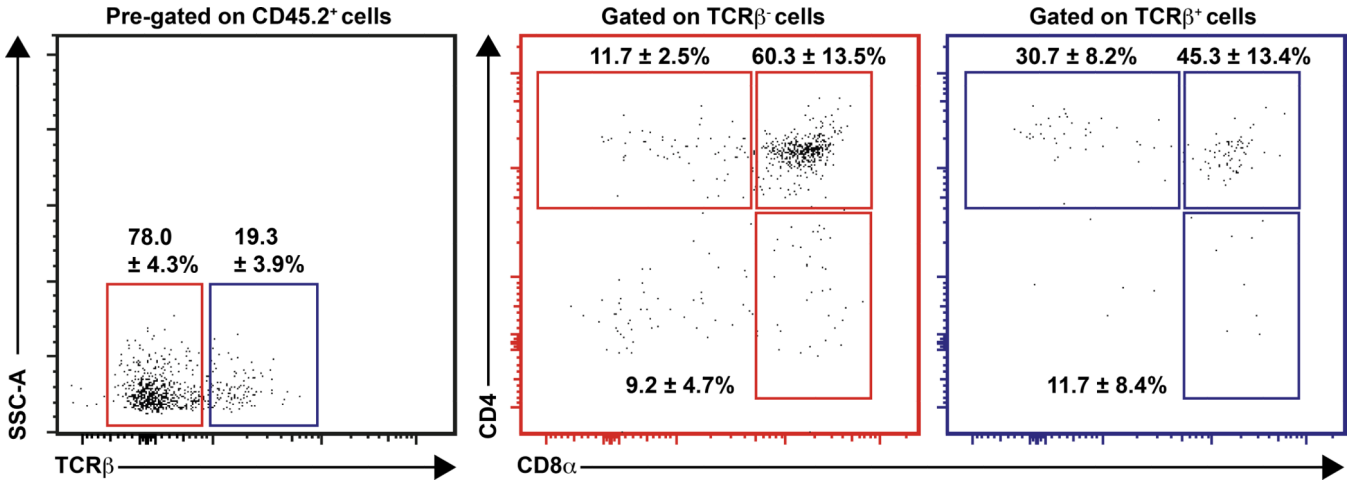

Figure 7. Extrathymic DPs differentiate into CD4$^+$ and CD8αβ$^+$ T cells

CD4$^+$CD8αβ$^+$TCR$^-$ cells (DPs) were isolated by flow cytometry from mediastinal adipose tissue and aortic arches of 10-week-old, female *C57BL/6J mice* (N=25 mice, N=8 pools of cells from 3–4 mice). E14 thymic lobes were dissected from *CD45.1/2 C57BL/6J mice* and cultured with 20000 extrathymic DPs in a hanging-drop culture. After 2 days, the thymic lobes were transferred into a submersion culture for 8 days and subsequently analyzed by flow cytometry. Representative flow cytometric plots of living extrathymic DPs in the fetal thymic organ culture. Frequencies of CD4$^+$ and CD8α$^+$ positive cells among TCRβ-positive (blue) and -negative cells (red) are reported.

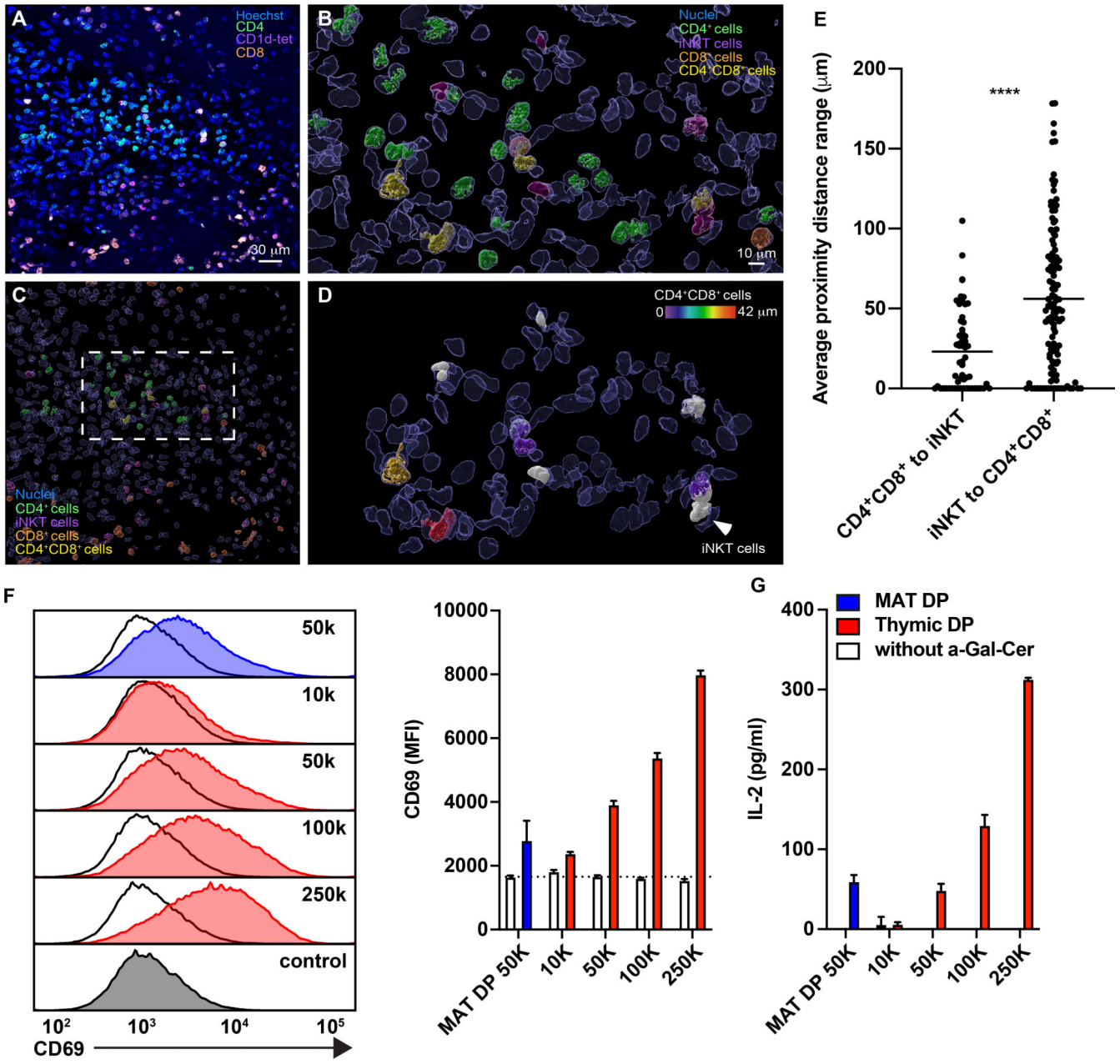

Figure 8. MAT DPs reside close to iNKT cells and can activate them.

(**A-D**) Whole mount mediastinal adipose tissue of an 8-week-old, female *C57BL/6J* mouse was stained for CD4 (green), CD8α (orange), alpha-GalCer:CD1d-tetramer (iNKT cells; purple/magenta), nuclei, (Hoechst; blue) and imaged using a C-APO 40x w (1.2) objective by confocal microscopy. (**B**) Rendered isosurfaces of labeled cells were constructed in IMARIS. $CD4^+$ cells (green), $CD8\alpha^+$ cells (orange), iNKT cells (purple/magenta), nuclei (blue), and $CD4^+CD8\alpha^+$ cells (yellow) are displayed. (**C**) Magnified area highlighted in (**D**). iNKT cells are highlighted in white. The distance of $CD4^+CD8\alpha^+$ cells to the closest iNKT cells is encoded by the color scale. (**E**) Ten independent regions of interest were analyzed for the distance between iNKT cells and $CD4^+CD8\alpha^+$ cells. Each with a fixed location of

one population to compare variable distance of the other from the cell center. (**F**) Thymic (red line) and MAT (blue line) $CD4^{+}CD8\alpha^{+}TCR^{-}$ cells were FACS sorted, pulsed with alpha-GalCer for 3.5 h or left untreated (black line), and co-cultured for 12h in duplicate with 50000 iNKT DN3A4-1.2 hybridoma cells. CD69 expression on the iNKT DN3A4-1.2 hybridoma cells was measured by flow cytometry (N=3/condition). A hybridoma control only was included (control) (**G**) Quantification of CD69 expression, dashed line represents expression of CD69 in the iNKT DN3A4-1.2 hybridoma only control. (**H**) The culture supernatant was analyzed for IL-2 levels by ELISA.